Assessing the Potential Impacts of Declining Arctic Sea Ice Cover on the Photochemical Degradation of Dissolved Organic Matter in the Chukchi and Beaufort Seas

Christie L. Logvinova[1], Karen E. Frey[1,*], Paul J. Mann[2], Aron Stubbins[3], Robert G. M. Spencer[4]

[1]*Graduate School of Geography, Clark University, Worcester, Massachusetts, USA*

[2]*Department of Geography, Northumbria University, Newcastle-upon-Tyne, NE1 8ST, UK*

[3]*Skidaway Institute of Oceanography, Department of Marine Science, University of Georgia, Savannah, GA, 31411, USA*

[4]*Department of Earth, Ocean and Atmospheric Science, Florida State University, Tallahassee, FL, 32306, USA*

[*]*Corresponding author: Email kfrey@clarku.edu ; Phone +1-508-793-7209*

Key Points:

- Photochemical degradability of western Arctic Ocean DOM was tested in a solar simulator
- Solar irradiation caused significant decreases in CDOM light absorption at UV wavelengths
- Continued declines in sea ice cover should result in enhanced CDOM photodegradation

Abstract

A warming and shifting climate in the Arctic has led to significant declines in sea ice over the last several decades. Although these changes in sea ice cover are well documented, large uncertainties remain in how associated increases in solar radiation transmitted to the underlying ocean water column will impact heating, biological and biogeochemical processes in the Arctic Ocean. In this study, six under-ice marine, two ice-free marine, and two ice-free terrestrially-influenced water samples were irradiated using a solar simulator for 72 hours (representing ~10 days of ambient sunlight) to investigate dissolved organic matter (DOM) dynamics from the Chukchi and Beaufort seas. Solar irradiation caused chromophoric DOM (CDOM) light absorption at 254 nm to decrease by 48 to 63%. An overall loss in total DOM fluorescence intensity was also observed at the end of all experiments, and each of 6 components identified by parallel factor analyses (PARAFAC) was shown to be photoreactive in at least one experiment. DOM fluorescence (FDOM) also indicated that the majority of DOM in under-ice and ice-free marine waters was likely algal-derived. Measurable changes in dissolved organic carbon (DOC) were only observed for sites influenced by riverine runoff. Losses of CDOM absorbance at shorter wavelengths suggest that the beneficial UV protection currently received by marine organisms may decline with the increased light transmittance associated with sea ice melt ponding and overall reductions of sea ice. Our FDOM analyses demonstrate that DOM irrespective of source was susceptible to photobleaching. Additionally, our findings suggest that photodegradation of CDOM in under-ice waters is not currently a significant source of carbon dioxide (CO_2) (i.e., we did not observe systematic DOC loss). However, increases in primary production and terrestrial freshwater export expected under future climate change scenarios may cause an increase in CDOM quantity and shift in quality throughout Arctic Ocean surface waters.

53 As arctic temperatures continue to warm and summer sea ice further declines, examination of the
54 resulting enhanced photodegradation processes and their impacts on the interplay between
55 primary production, carbon cycling, and surface ocean heating processes will be paramount.
56
57 **Index Terms and Keywords:** 0793, 0428, 0475, 0750, 1621; Chromophoric Dissolved Organic
58 Matter (CDOM), Dissolved Organic Carbon (DOC), Light Absorption, Arctic, Sea Ice,
59 Photodegradation
60
61 **1. Introduction**
62 Recent climate warming has caused significant decreases in sea ice extent across the Arctic
63 [*Serreze et al*., 2007; *Stroeve et al*., 2007; *Comiso et al*., 2008], with a record minimum in
64 September 2012 that was 49% below the 1979–2000 average [*Perovich et al*., 2012]. Over the
65 past three decades, there has also been an increase in the length of the summer melt season
66 [*Markus et al.*, 2009] and an increasing percentage of thin first-year ice as compared with thicker
67 multi-year ice [*Maslanik et al*., 2007, *Kwok and Rothrock*, 2009; *Maslanik et al*., 2011; *Comiso*,
68 2012]. Declining sea ice extent reduces surface albedo, thereby enhancing the amount of solar
69 radiation absorbed by associated ocean waters and ice. Furthermore, melt ponds form more
70 easily and cover more surface area on thin first-year ice than on multi-year ice [*Fetterer and*
71 *Untersteiner*, 1998; *Nicolaus et al.,* 2012], and light transmittance through these melt ponds can
72 be up to an order of magnitude greater than through unponded sea ice [*Light et al*., 2008; *Frey et*
73 *al*., 2011, *Nicolaus et al*., 2012]. In future climate scenarios, Arctic sea ice is expected to
74 continue thinning, decreasing in areal extent, and increasing its melt-pond coverage [*Wang and*
75 *Overland*, 2009; *Schröder et al*., 2014], yet large uncertainties remain in how the resulting

increase in solar radiation transmitted to the underlying ocean waters will impact biological and biogeochemical processes in the Arctic Ocean.

A major uncertainty linked to sea ice decline is to what extent dissolved organic matter (DOM) in underlying ocean waters will be impacted. In the Arctic Ocean, DOM primarily results from either: (a) *in situ* biological production in the upper water column and within sea ice; or (b) inputs of terrestrially-derived organic matter transported to the ocean by fluvial systems [*Carlson*, 2002; *Holmes et al*., 2012; *Raymond and Spencer*, 2015]. Chromophoric DOM (CDOM) is the optically active fraction of this dissolved material, absorbing ultraviolet (UV) and visible light, and acting as one of the primary regulators of light penetration in surface waters [*Blough and Del Vecchio,* 2002; *Nelson and Siegel,* 2002]. CDOM regulates the amount of photosynthetically active radiation (PAR) in the water column, which influences the rates and distribution patterns of primary production [*Retamal et al.,* 2008]. CDOM also efficiently blocks UV radiation, thereby protecting marine organisms from DNA damage and other harmful effects [*Williamson et al.,* 2001]. By absorbing shortwave visible radiation (380–760 nm), CDOM can additionally contribute to the heating of surface waters and subsequent melting of sea ice [*Kirk,* 1988, 1994; *Pegau*, 2002; *Granskog et* al., 2007; *Hill,* 2008]. The absorption of light by CDOM can lead to photodegradation of DOM [*Mopper et al*., 2015], generally resulting in a decrease in CDOM absorption (i.e., photobleaching; *Helms et al.,* 2008; 2014). Through these photodegradation processes, a pool of DOM can be directly photomineralized to inorganic carbon, with subsequent outgassing of CO_2 to the atmosphere [*Stubbins et al*., 2008; *Powers and Miller,* 2015]. In addition, photochemical alteration of DOM influences the bioavailability of residual DOM to aquatic bacteria [*Moran and Zepp*, 1997; *Bittar et al*., 2015]. The presence and

99 characteristics of arctic sea ice can therefore play a critical role in determining light penetration,
100 in turn influencing CDOM distribution and biogeochemical cycling in surface ocean waters.
101
102 Over the past ~30 years, the Chukchi and Beaufort seas of the western Arctic have experienced
103 some of the greatest declines in sea ice extent across the Arctic Ocean [*Comiso et al*., 2008],
104 exposing the marine environment in this region to continually increasing amounts of solar
105 radiation [*Perovich et al*., 2007]. To date, only a few studies have investigated DOM in the
106 western Arctic Ocean, with these typically focusing on the distribution of CDOM in open waters
107 [*Gueguen et al*., 2005, 2007, *Retamal et al*., 2007; *Matsuoka et al*., 2007, 2011; *Hill*, 2008;
108 *Walker et al*, 2009]. Furthermore, given the heavily riverine-influenced nature of the Arctic
109 Ocean [*Opsahl et al*., 1999; *Dittmar and Kattner*, 2003], DOM photoreactivity studies have
110 focused primarily on terrigenous DOM in the coastal regions [*Belanger et al*., 2006; *Osburn et*
111 *al*., 2009]. Thus, despite the critical need to understand the impacts of a shrinking and thinning
112 sea ice cover, to the best of our knowledge this work represents the first study to focus upon the
113 photoreactivity of DOM beneath sea ice. In this study, we used a series of controlled laboratory-
114 based photodegradation experiments to investigate DOM dynamics in under-ice ocean waters
115 collected from the Chukchi and Beaufort seas during the summer of 2011. Absorbance and
116 fluorescence spectroscopy were used to identify the likely source of DOM, and to trace changes
117 in CDOM optical properties during photochemical degradation. These results were then
118 examined alongside changes in dissolved organic carbon (DOC) concentration to assess the
119 relative importance of photobleaching and photomineralization. Finally, we discuss the potential
120 photochemical susceptibility of Arctic Ocean DOM and how future changes to sea ice may

influence primary productivity, carbon biogeochemistry, and the heat balance in the Arctic Ocean.

2. Methods

2.1. Sample Collection

Sampling took place during the NASA Impacts of Climate Change on the Eco-Systems and Chemistry of the Arctic Pacific Environment (ICESCAPE) mission in the Chukchi and Beaufort seas during the summer melt season in July 2011 on the US Coast Guard Cutter (USCGC) *Healy*. Water samples were collected from 10 locations distributed across three north-south transects (Figure 1). The westernmost transect was located on the continental shelf of the Chukchi Sea (IFM_1 and $ICM_{1–3}$). The central transect crossed the shelf-basin interface in the Chukchi Sea (IFM_2 and $ICM_{4–5}$). The easternmost transect extended into a region of the Beaufort Sea basin impacted by river runoff, primarily from the Colville River ($IFT_{1–2}$ and ICM_6).

At six ice-covered stations ($ICM_{1–6}$; Figure 1), water samples were collected from directly below the ice at the ice-water interface by hand-deploying a 2 L Kemmerer (vertically oriented) water sampler. At the remaining 4 stations located in open water, surface water samples were collected using the ship's CTD rosette, which consisted of a 12-place rosette with 30 L Niskin bottles. Two of these stations were located near the ice edge ($IFM_{1–2}$; Figure 1) and two were from surface waters likely influenced by the Colville River ($IFT_{1–2}$). Salinity measurements for each sample were made onboard using a Guildline Autosal salinometer. Immediately after sampling, water samples for photodegradation experiments were filtered through a pre-rinsed 0.2 μm filter (Whatman PolyCap) and transferred into acid washed (10% HCl) precombusted (450°C for 6

144 hours) Kimax glass bottles. Samples were kept frozen (-20°C) and dark until return to the
145 laboratory.
146
147 **2.2. Photodegradation Experiments**
148 After slowly thawing overnight, water samples were transferred into acid-washed (10% HCl),
149 precombusted (450°C for 6 hours) round bottom quartz flasks (70 ml; Quartz Scientific Inc., OH,
150 USA) and closed with ground-glass stoppers to exclude air bubbles. Flasks were rinsed with
151 sample water three times prior to filling and then placed bottom side up in a 20°C water bath
152 containing Milli-Q water. Samples were positioned just under the water surface. The bath was
153 mounted inside an Atlas Suntest XLS+ solar simulator fitted with an Atlas NXe 1700w bulb and
154 daylight filter, to provide a light spectrum similar to that of natural sunlight between 280 and 800
155 nm. Total lamp power was 765 W m^{-2} with a constant exposure of 65 W m^{-2} between 300 to 400
156 nm. Samples were exposed for 72 hours, receiving a radiant exposure of 16,865 ± 6.7 kJ m^{-2} of
157 energy (time integral of spectral irradiance), equivalent to approximately 10 days of ambient
158 sunlight during the summer months at 70°N (based on the System for Transfer of Atmospheric
159 Radiation (STAR) [*Ruggaber et al*., 1994] and following adaptations described in *Powers and*
160 *Miller* [2015].). CDOM, fluorescent DOM (FDOM) and DOC were measured (details below) at
161 the beginning of the experiment and then again after 4, 12, 24, and 72 hours of light exposure.
162 Triplicate samples and a single dark control (treated identically but wrapped in foil) were used at
163 all time points, with triplicate dark controls for the initial and final (72-hour) time points.
164
165
166

167 **2.3. CDOM Analysis**

168 CDOM absorbance was measured using a Shimadzu UV-1800 UV-Visible spectrophotometer at
169 1 nm intervals between 800 and 200 nm using a 10 cm quartz cuvette. All sample spectra were
170 blank corrected and referenced against Milli-Q water (18.2 Ω)**.** In order to minimize temperature
171 effects, all measurements were made after samples had equilibrated to laboratory temperature.
172 CDOM absorbance was assumed to be zero above 750 nm, therefore the average sample
173 absorbance between 750 nm and 800 nm was subtracted from the spectrum to correct for offsets
174 owing to instrument baseline drift, temperature, scattering and refractive effects [*Green and*
175 *Blough*, 1994; *Helms et al*, 2008]. CDOM absorption coefficients were calculated from:
176
177 $$a(\lambda) = 2.303A(\lambda)/l \quad (1)$$
178
179 where a is the Naperian light absorption coefficient (m^{-1}) at λ (the wavelength in nanometers), A
180 is the absorbance at λ wavelength, and l is the cell path length in meters [*Green and Blough*,
181 1994].
182
183 Spectral slopes (S, nm^{-1}) for each CDOM absorbance spectrum were derived using an
184 exponential function:
185
186 $$a(\lambda) = a(\lambda_0)e^{-S(\lambda-\lambda_0)} \quad (2)$$
187
188 where $a(\lambda)$ is the absorption coefficient of CDOM (m^{-1}) at wavelength λ and λ_0 is the reference
189 wavelength. Spectral slopes were calculated across the wavelength ranges of 275–295 nm and

350–400 nm. Spectral slope parameters can provide information pertaining to DOM molecular weight, photochemical processing and source [*Blough and Del Vecchio*, 2002; *Helms et al.,* 2008], and have been found to be largely independent of CDOM concentration [*Brown,* 1977]. The 275–295 nm and 350–400 nm slope ranges were chosen as they have been shown to contain the greatest variation in a wide range of samples, including DOM-rich terrestrial, estuarine, coastal and highly photobleached waters [*Helms et al.,* 2008; *Spencer et al.*, 2012]. The ratio of these slopes (S_R) has been shown to be particularly sensitive to changes in molecular weight and was calculated by dividing $S_{275–295}$ by $S_{350–400}$ [*Helms et al.,* 2008]. All slopes are reported as positive numbers such that higher (i.e., steeper) slopes indicate a greater decrease in absorption with increasing wavelength.

2.4. FDOM Analysis

The fluorescent portion of CDOM (FDOM) was characterized using fluorescence excitation emission matrix (EEM) spectroscopy, which creates three-dimensional structures composed of multiple emission spectra at a range of excitations and provides additional information about the chemical composition and sources of CDOM [*Coble*, 1996; 2007; *Stedmon et al*., 2003; *Stubbins et al*., 2014]. FDOM measurements were collected on a FluoroMax 4 spectrofluorometer (Horiba Jobin-Yvon). EEMs were obtained by recording sample emission across 320 to 500 nm (with 2 nm increments) after excitation from 250 to 450 nm wavelengths (with 5 nm increments). A single sample EEM was collected at each time point (0, 4, 12, 24, and 72 hours). Owing to low fluorescence intensities, samples were run using long integration periods (0.5 s) to minimize measurement noise. All EEMs were blank corrected and Raman calibrated [*Lawaetz and Stedmon,* 2009; *Murphy et al*., 2010] using Milli-Q water spectra run on the same day. Finally, to

eliminate Rayleigh scattering effects, zeroes were inserted in the region where emission wavelengths are less than or equal to the excitation wavelength (+30 nm). The absorption coefficients of all samples were <10 m^{-1}, eliminating the need for inner filter corrections [*Stedmon and Bro*, 2008; *Murphy et al*., 2010].

Many fluorescent components have overlapping peaks making it difficult to identify individual components within an EEM. To identify independently varying FDOM components within our dataset, and to assess changes in marine- vs. terrestrially-derived material, we conducted parallel factor analyses (PARAFAC) in MATLAB using the DOMFluor Toolbox following the methods as outlined in *Stedmon and Bro* [2008]. In total, we included 50 EEMs containing 5 different time points for each of the 10 experiments. By tracing processes using time-series measurements of FDOM, PARAFAC modeling may yield more meaningful results than if applied to discrete samples [*Stedmon & Bro*, 2008]. To simplify the modelling process and minimize noise, we included only emission wavelengths from 320 to 476 nm in the EEMs. No EEMs were identified as outliers. A series of PARAFAC models (utilizing between 2 to 7 components) were applied and initial model fitting assessed using the steps as outlined in *Stedmon & Bro* [2008]. Final model validation was conducted using a range of techniques including random split half analysis and random initialization [*Stedmon & Bro*, 2008]. Split half validation involves splitting the sample data into two halves and comparing model fits after running models on the two halves independently. Random initialization was then used to ensure that the models were in fact the least squares result and represented local minima.

236 **2.5. Dissolved Organic Carbon Analysis**

237 After the experiments, samples for DOC analyses were acidified (pH < 2) by addition of HCl and
238 analyzed for non-purgable organic carbon using a Shimadzu TOC-VCPH analyzer fitted with a
239 Shimadzu ASI-V autosampler. Standards were prepared by the volumetric dilution of a stock
240 solution containing 500 μM-DOC (potassium hydrogen phthalate, p.a.) to produce the following
241 series of standards: 0, 2, 5, 8, 10, 25, 50, 75, 100 μM-DOC. In addition to standards, aliquots of
242 deep seawater reference material (Batch 10, Lot# 05-10) from the Consensus Reference Material
243 Project (CRM) were analyzed to ensure the precision and accuracy of the DOC analyses.
244 Analyses of the CRM deviated by less than 5% from the reported value for these standards (41 to
245 44 μM-DOC; http://yyy.rsmas.miami.edu/groups/biogeochem/Table1.htm). Standard and sample
246 volumes analyzed were 20 to 40 mL. Routine minimum detection limits in the investigators
247 laboratory using the above configuration are 2.8±0.3 μM-C and standard errors are typically 1.7
248 ±0.5 % of the DOC concentration [*Stubbins and Dittmar*, 2012].
249
250 **3. Results**
251 **3.1. Photodegradation of CDOM**
252 Photodegradation experiments were conducted on waters from 10 separate stations across the
253 Chukchi and Beaufort seas. Figure 2 shows absorption coefficient spectra over the course of a
254 72-hour experiment (including triplicate analyses for each time step) for a typical ice-covered
255 marine (ICM_1), ice-free marine (IFM_1), and ice-free terrestrially-influenced (IFT_1) sample.
256 CDOM measurements from replicate samples at each individual time step and experiment
257 demonstrated little between-flask variability (with a coefficient of variance <0.06 at 254 nm for
258 all experiments). Therefore, from here on we present only sample means of triplicate

259 measurements. All under-ice ($ICM_{1–6}$) and marine samples ($IFM_{1–2}$) had lower initial CDOM
260 absorption values (ranging from 1.36 to 2.17 m^{-1} at 254 nm) than terrestrially-influenced ($IFT_{1–2}$)
261 samples (3.12 to 5.79 m^{-1} at 254 nm). Despite these initial differences, CDOM from all 10
262 stations was found to be photoreactive (Table 1, Figure 3a). For all experiments,
263 photochemically induced changes in the absorption coefficient at 254 nm (a_{254}) over the 72-hour
264 period were found to be statistically significant ($p < 0.05$; two-tailed Student's t-test on triplicate
265 samples from the beginning and end of each experiment) with total losses in a_{254} of between 48
266 and 63%. No significant differences were observed between initial a_{254} values and those of the
267 dark controls after 72 hours ($p < 0.05$) across any of the experiments, confirming photochemical
268 processes led to the observed reductions in absorbance. With the exception of samples ICM_5 and
269 IFM_1, sample waters also showed statistically significant photobleaching at 365 nm (a_{365}), with a
270 greater decrease observed in the IFT samples than in the marine samples (Table 2). Initial
271 absorption coefficients at 440 nm (a_{440}) were relatively low (most were at or below the detection
272 limit of the spectrophotometer (±0.002 absorbance or 0.05 m^{-1})) and losses in a_{440} were not
273 statistically significant for 7 of the 10 experiments (Table 2).
274
275 CDOM absorption values at 254 nm for the marine samples, whether from under-ice (ICM) or
276 ice-free (IFM) waters, were not significantly different from one another (at both initial and final
277 time points), yet both were statistically different ($p < 0.05$) from terrestrially-influenced samples.
278 Overall, the marine samples had lower initial a_{254} values (mean for ICM and IFM = 1.65 m^{-1})
279 and exhibited smaller decreases in a_{254} (mean = 0.88 m^{-1}) as compared to the terrestrially-
280 influenced samples (mean a_{254} = 4.46 m^{-1}, showing a mean loss of 2.63 m^{-1}, Table 2) .
281

As samples were not all optically thin, to more accurately determine changes in the efficiency of photobleaching between samples, the CDOM absorption coefficient was additionally plotted as a function of cumulative UV light (280–400 nm) absorbed (Figure 3b). The range of 280–400 nm was chosen because these are quantitatively the most important wavelengths for environmental photoreactions involving CDOM [*Mopper et al*., 2015]. The decrease in the CDOM absorption coefficient at 254 nm was approximately exponential and could be modeled using the following three-parameter exponential decay equation:

$$C(u) = C_{\infty} + z_0 e^{-ku} \quad (3)$$

where u is cumulative UV light absorbed in kW/m^2, C*(u)* is the modeled absorption coefficient, C_{∞} is the non-photoreactive component, z_0 is the photoreactive component, and k is the rate of decay. The exponential decay models fit the experimental results well with adjusted R^2 values ranging from ~0.94 to 0.98 for all experiments (Table 3). Overall, marine samples had smaller photoreactive components (z_0) and residual nonphotoreactive (C_{∞}) components compared to the terrestrially influenced samples. Additionally, the rate of decay (k) was greater for marine samples compared to the terrestrially-influenced samples, with the exception of IFM_2 which had a rate of decay similar to IFT_2. There is also a strong relationship (adjusted $R^2 = 0.99$) between the initial absorption coefficient (C(0)) and the photoreactive component (z_0) (Figure 4).

Changes in DOM composition were also apparent during the 72-hour irradiation experiments with clear shifts in the spectral slope parameters. For all experiments, $S_{275–295}$ decreased within the first 6 hours of irradiation, and then showed either little change, or a slight increase at

subsequent time points (Figure 5a). For most of the experiments, $S_{350–400}$ decreased over time or showed little change (Figure 5b). Over the full length of the experiment, 9 of the 10 experiments (except IFT_1) showed a statistically significant decrease ($p < 0.5$; two-tailed Student's t-test on triplicate samples from the beginning and end of each experiment) in $S_{275–295}$ (Table 4). For $S_{350–400}$, 9 of the 10 experiments (except ICM_5) also showed a statistically significant ($p < 0.5$) decrease (Table 4). Of the experiments that had a statistically significant change in S_R, all increased over the course of the experiment with the exception of ICM_6 (Table 4).

3.2. Photodegradation of FDOM and PARAFAC results

An overall loss in total DOM fluorescence intensity was observed at the end of all experiments. Figure 6 shows EEMs from four representative experiments (ICM_1, IFM_1, IFT_1, IFT_2) during the 72-hour irradiation period. Under-ice marine samples had consistently lower initial FDOM intensities as compared to ice-free marine and terrestrially-influenced samples. Furthermore, a greater proportion of the fluorescence signal was typically present at emission wavelengths less than 400 nm in the ICM and IFM samples, relative to the terrestrially-influenced sites. The two terrestrially-influenced samples clearly contained additional fluorescence signatures dominated by broad fluorescence peaks at emission wavelengths greater than 400 nm. Although all ten samples showed an overall decay in FDOM intensity over the 72-hour experiments, several samples showed an increase in total fluorescence intensity at intermediary time points (e.g. sample IFT_2 at t_4 in Figure 6), which then subsequently decayed.

Six independent fluorescent components were validated using PARAFAC analysis (Figure 7). Owing to the complex nature of DOM, it is unlikely that these components represent single

328 fluorophores, but instead represent a group of fluorophores that have similar properties and
329 variability within the dataset (*Baker and Spencer*, 2004; *Murphy et al*., 2010; *Stubbins et al*.,
330 2014). In particular, component 5 exhibited a shoulder that indicates that this component likely
331 represents a mixture of fluorophores that the model was not able to separate because they co-
332 varied in the dataset [*Stedmon and Markager,* 2005a]. The excitation and emission spectra of the
333 components derived here are statistically compared to previously identified components in the
334 OpenFluor database using the Tucker congruence coefficient in order to identify potential
335 sources for each (*Murphy et al.*, 2014b; Table 5). Components 1,3,4 and 5 were statistically
336 similar to other components in the database and components 2 and 6 resembled components
337 found in other studies (Table 5).
338
339 Components 1, 2 and 6 had spectra resembling humic-like DOM, with broad emission spectra
340 around and above 400 nm and a broader excitation spectra compared to the other components
341 (Figure 7). Components 1 and 2 exhibit characteristics of humic-like terrestrially-derived
342 material [*Stedmon and Markager*, 2005a, b; *Stedmon et al.*, 2007a; *Kowalczuk et al*., 2009;
343 *Yamashita et al*., 2010b; *Jørgensen et al*., 2011; *Murphy et al.,* 2011; *Seredynska-Sobecka et al*,
344 2011; *Shutova et al.*, 2014; *Tanaka et al*., 2014]. Component 6 has also been identified as humic-
345 like [*Stedmon and Markager*, 2005a; *Stedmon et al*., 2007a; *Stedmon et al*., 2007b; *Yamashita et*
346 *al*., 2010a; *Jørgensen et al*., 2011] and *Stedmon and Markager* [2005a] categorized it as marine
347 derived or anthropogenic in nature. Components 3, 4 and 5 exhibited spectra resembling
348 'protein-like' DOM, with emission spectra maxima below 400 nm. Component 3 most closely
349 resembles amino acids, free or bound in proteins [*Murphy et al*., 2008; 2014a] and component 4
350 resembles tyrosine [*Yamashita et al.,* 2011*; Graeber et al*., 2012; *Yamashita et al.,* 2013], both of

which are considered to be primarily microbially derived in marine waters [*Stedmon and Markager*, 2005b; *Coble*, 1996]. Component 5 is more difficult to classify, however, it is similar to component 6 in *Jørgensen et al*. [2011] that has been previously linked to surface water productivity.

Terrestrially-influenced samples IFT_1 and IFT_2 had the highest overall fluorescence at the beginning of the experiments and were largely dominated by the humic-like component 1 (29–40% of initial fluorescence; Table 6). The IFM_1 sample was initially dominated by component 5 (48%) and also contained high levels of the protein-like components 3 (22%) and 4 (20%). The IFM_2 and under-ice samples generally exhibited low initial FDOM intensities with no clearly dominant fluorescent component. The exception was ICM_6, which exhibited greater contributions from component 4 (56%).

Distinct similarities and differences between sample types were observed with respect to how components changed over the 72-hour irradiation experiments (Figure 8, Table 6). In general, under-ice marine waters exhibited only small changes in each component with irradiation (typically less than 0.03 r.u.). For the ice-free marine samples, IFM_1 exhibited large changes in fluorescence in the three protein-like components, whereas IFM_2 showed little change in any component. For the terrestrially-influenced samples, IFT_1 showed large losses in each component (55–99%) and IFT_2 exhibited large declines in components 2, 3, 4, and 5 (50–83%). Both IFT_1 and IFT_2 showed the greatest losses in 'humic-like' components 4 and 5 (80–99%).

374 **3.3 Photomineralization of DOC**

375 DOC concentrations from the beginning and end of nine of the experiments are shown in Table 1
376 (sample loss prohibited measurement on the IFM_1 sample). Initial DOC concentrations in ICM
377 and IFM samples were relatively low (53.6–71.9 μM), with higher concentrations in the two
378 terrestrially-influenced samples (105.4 and 80.5 μM). There was no apparent relationship
379 between salinity and DOC. Of the nine experiments, only three (ICM_6, IFT_1, and IFT_2) showed a
380 statistically significant ($p < 0.05$) change in DOC at the end of the 72-hour irradiation period.
381 Photomineralization losses were greatest in river-influenced samples, which showed an 8%
382 (IFT_1) and 7% (IFT_2) decrease from initial DOC concentrations. The under-ice marine sample
383 ICM_6 showed a 3% loss of DOC over this period. Overall losses in CDOM were far greater than
384 for DOC (Figure 9a). In particular, the percent loss in a_{254} ranged from ~48 to 62%, whereas the
385 percent loss in DOC was only ~0 to 8% (Figure 9b).
386
387 **4. Discussion**

388 **4.1. Impact of Photodegradation on CDOM from Sea-Ice Melt**

389 Initial CDOM absorption values were lower in ICM and IFM samples than in terrestrially-
390 influenced samples, in good agreement with many previous studies that report typically higher
391 CDOM absorption in coastal, river-influenced regions than in open ocean regions [*Blough and*
392 *Del Vecchio*, 2002; *Kitidis et al*., 2006; *Osburn et al*., 2009]. CDOM in the water column has
393 been shown to be excluded from sea ice during formation [*Amon,* 2003]. Therefore, in the
394 absence of sea ice algae producing CDOM *in situ* [*Scully and Miller*, 2000], it would be expected
395 that CDOM within sea ice melt would be low as well. The range in initial CDOM absorption
396 values for ICM and IFM samples (1.36–2.17 m^{-1}) could be partially explained by the range in

397 salinity (17.4–31.7), which suggests that DOM in these surface waters was of various sources
398 and likely variable ages and residence times and therefore had undergone varying amounts of
399 photochemical degradation prior to sampling. Despite differences in initial CDOM absorption
400 values, CDOM was shown to be photoreactive irrespective of sampling location. Continuous
401 losses of absorbance at 254 nm were observed (Figure 3a), suggesting photochemical exposure
402 caused the average aromatic content of the DOM pool to be progressively reduced during
403 irradiation [*Osburn et al*., 2001; *Stubbins et al*., 2010; *Helms et al*., 2014].
404
405 Photobleaching kinetics for a_{254} in these experiments are well described by three parameter
406 exponential decay models. Based on the photoreactive component (z_0) predicted to be lost after
407 infinite photo-exposure by these models, a_{254} could decrease by at least half for almost all of the
408 samples if exposed to the sun indefinitely, indicating that UV absorption by CDOM at these
409 shorter wavelengths is diminished by photodegradation. However, these models indicated that,
410 regardless of sample type or initial CDOM values, residual amounts (C_∞) of a_{254} (~0.57–0.91 m^{-1}
411 for under-ice and ice-free marine samples, and 1.36 and 1.63 m^{-1} for the two terrestrially
412 influenced samples) would survive infinite photo-exposure, suggesting a persistent, yet small
413 fraction of non-photoreactive DOM (that absorbs shortwave UV) was present in all waters.
414 Additionally, there is also a strong relationship (adjusted $R^2 = 0.99$) between the initial
415 absorption coefficient (C(0)) and the photoreactive component (z_0) of all sample types (Figure 4)
416 indicating that final a_{254} could potentially be predicted from initial measurements based on a
417 regional model.
418

In our experiments, samples demonstrating significant changes in the spectral slope parameter, generally exhibited decreases in both $S_{275–295}$ and $S_{350–400}$, and an increase in S_R during irradiation. For $S_{275–295}$ in particular, much of the change occurred within the first 6 hours of the 72-hour irradiation (Figure 5a) indicating rapid initial photo-alteration in DOM composition. Similar to our experiments, *Helms et al.* [2008] showed increases in S_R and decreases in $S_{350–400}$, however they showed that $S_{275–295}$ increased during their photodegradation experiments. In another study, *Spencer et al.* [2009] showed that (despite an initial increase in $S_{275–295}$) $S_{275–295}$ values decreased in Congo River DOM during irradiation after extensive light exposure. We suggest therefore that the decreases in $S_{275-295}$ in most of our samples may have been caused by extensive prior photo-degradation in the environment, although these optical patterns may also derive from the freshly-produced algal nature of CDOM in sea ice impacted waters. For example, irradiation of CDOM from algal cultures can result in $S_{275-295}$ becoming shallower during photobleaching [*Bittar et al.* 2015]**.** Changes in spectral slope parameters during irradiation have been related to changes in mean molecular weight [*Helms et al.,* 2008], where there have been particularly strong relationships between increases in S_R and decreases in average DOM molecular weight. Five of our experiments (ICM_1, ICM_3, ICM_4, IFM_2, IFT_1) showed a significant increase in S_R during exposure. Based upon these results our samples may have undergone a significant decrease in mean DOM molecular weight during irradiation. However, the work by *Helms et al.* [2008] looked at samples across a strong terrigenous-to-marine DOM gradient in the Southeastern US, far from the current study site in terms of geography and biogeochemical system. Therefore, inferences about DOM quality based upon spectral slope and S_R in our current system must be interpreted with due caution until work

441 shows that CDOM spectral qualities have similar empirical relationships to DOM quality in high
442 latitude, sea ice impacted surface waters.
443
444 **4.2. Impact of Photodegradation on FDOM from Sea-Ice Melt**
445 A greater relative proportion of fluorescence at emission wavelengths less than 400 nm was
446 typically present in each of the under-ice and ice-free marine samples, as compared to the
447 terrestrially-influenced sites. This is often referred to as 'protein-like' fluorescence, has
448 commonly been reported in marine samples [*Coble*, 1996; *Stedmon and Markager*, 2001], and
449 appears to be associated with a family of low molecular weight molecules, including aliphatics
450 and nitrogen-enriched aromatics [*Stubbins et al*., 2014]. The two terrestrially-influenced samples
451 contained fluorescence signatures dominated by broad fluorescent peaks at emission wavelengths
452 greater than 400 nm. This is typical of waters influenced by river runoff and commonly referred
453 to as 'humic-like' fluorescence [*Coble*, 1996; *Stedmon and Markager*, 2001; *Fellman et al*,
454 2010]. These signatures have been associated with nitrogen-poor, relatively high mass molecular
455 families [*Stubbins et al*., 2014]. All ten samples show an overall decay in FDOM intensity over
456 the 72-hour experiments, with the exception of protein-like production in several samples
457 (occurring after 4 hours in sample IFT_2, Figure 5), which subsequently decayed. Photo-induced
458 production of tyrosine-like fluorescence (which contributes to the protein-like fluorescence
459 signal) has been previously observed in lacustrine [*Stedmon et al*., 2007a] and marine waters
460 [*Mann*, 2010].
461
462 PARAFAC decomposition identified 6 components and overall, these fluorescent components
463 were shown to decay, or remain constant, over the course of the experiments. Under-ice and ice–

free marine waters were dominated by the protein-like components, whereas terrestrially influenced samples contained higher proportions of the humic-like fluorophores (Figure 8 and Table 5). All components were shown to be photoreactive in at least one of our experiments, further demonstrating that DOM irrespective of source was susceptible to photobleaching. Under-ice and ice-free marine waters showed the greatest decreases in FDOM of protein-like components (which are associated with recently algal-produced labile DOM), whereas the greatest decreases in the terrestrially-influenced samples occurred in humic-like components.

Studies have indicated that photo-degradation of DOM can result in increasing [*Moran and Zepp*, 1997] or decreasing biological lability [*Tranvik and Kokalj*, 1998] depending on DOM source. In general, both field and laboratory studies suggest that photodegradation causes humic-rich DOM to become more bioavailable whereas recently produced algal-derived DOM in surface waters becomes less biolabile [*Benner and Biddanda*, 1998; *Obernosterer et al.,* 1999; 2001; *Tranvik et al*., 1999; *Tranvik and Bertilsson,*2001; *Bittar et al.*, 2015]. In particular, protein-like fluorescence of algal origin has been shown to be both biolabile and photolabile, indicating these two processes compete to mineralize fresh, algal DOC (*Stedmon and Markager*, 2005b; *Bittar et al.*, 2015). Based on our FDOM analyses, the majority of CDOM in under-ice and ice-free marine waters appears to be algal-derived, therefore we may expect photoirradiation of these waters to reduce the availability of biolabile DOC through direct photo-mineralization and through photo-alteration to less biolabile material as found for DOM produced by algal cultures [*Bittar et al.,* 2015]**.** Thus, photochemistry of algal-derived DOM in sea ice systems may short-circuit the microbial loop, whereas photo-degradation of terrigenous DOM is likely to increase DOM biolability and enhance bacterioplankton productivity.

487 **4.3. Photobleaching vs. Photomineralization**

488 Three of our samples displayed significant changes in DOC concentration with irradiation. The
489 three samples (ICM_6, IFT_1 and IFT_2) were all from the easternmost transect that was closest to
490 the mouth of the Colville River and were likely influenced by the relatively high-DOC, high-
491 CDOM riverine water runoff. Investigating the various components identified in the PARAFAC
492 analysis, changes in component 2 (identified as humic-like and terrestrially-derived; Table 5) had
493 the strongest significant correlation with changes in DOC ($R = 0.78$, $p < 0.02$) indicating that
494 there may be a link between this component and DOC. These results suggest that as melt ponds
495 form and sea ice retreats, terrestrial DOM below the ice would be susceptible to
496 photomineralization to dissolved inorganic carbon.
497
498 Our experiments suggest that it is not possible to calculate DOC from CDOM using a constant,
499 linear relationship in the Chukchi and Beaufort seas. Several methods for using CDOM
500 measurements as a proxy for DOC have previously been proposed [*Ferrari et al*., 1996; *Del*
501 *Vecchio and Blough*, 2004; *Guéguen et al*., 2005] because CDOM can be measured at a much
502 higher spatial resolution using remote sensing and at a high temporal resolution using *in situ*
503 measurements, and as such, it has the potential to more easily provide broader spatial and
504 temporal coverage. A promising new approach was suggested by *Fichot and Benner* [2011],
505 which derives DOC concentrations from CDOM absorption coefficients at 275 and 295 nm and
506 their approach worked well for the coastal waters of the Beaufort Sea (eastward of our study
507 area). However, based on the results of our photodegradation experiments, the method is likely
508 not applicable for the nearby under-ice and ice-free marine waters (that are less influenced by

509 river runoff) as while there were measurable changes in the absorption coefficients at shorter
510 wavelengths with irradiation, there were no measurable changes in DOC.
511
512 Photodegradation resulted in measurable changes in the optical properties of DOM in all sample
513 waters, yet none of the ice-free and under-ice marine samples from the westernmost and central
514 transects showed a significant change in DOC with irradiation. Several studies have shown that
515 photochemical loss of DOC is less efficient than CDOM photobleaching [*Moran et al.*, 2000;
516 *Vahatalo and Wetzel*, 2004; *Spencer et al*., 2009]. Furthermore, *Osburn et al.* [2009] conducted
517 photoreactivity experiments on water samples from the Mackenzie River, estuary, shelf and gulf
518 regions of the western Canadian Arctic and found less than 1% loss in DOC after 3 days in
519 ambient arctic sunlight. Similar results were found for sea ice brine from Antarctic sea ice
520 [*Norman et al*., 2011]. The absence of measurable changes in DOC in waters in the westernmost
521 and central transects in this study indicates that either there is a decoupling between CDOM
522 photobleaching and DOC photomineralization or that any changes in DOC were below the
523 detection limit of our instrument.
524
525 Photochemistry can result in the production of CO_2 through two different pathways: (a) the
526 abiotic photomineralization of DOC into CO_2 and CO; and (b) a photochemical-biotic pathway
527 through which photodegradation alters the bioavailability of DOM potentially making it more
528 labile allowing it to be consumed by bacteria and converted into biomass and CO_2 [see sources in
529 *Mopper et al.*, 2015]. Not only was there very little photomineralization evident in the western
530 and central transects in our study, but the changes in spectral slopes and fluorescence
531 components observed in these experiments suggest that there may have been an overall reduction

532 in the biolability of DOM in under-ice and marine surface waters. Therefore, it appears that
533 photodegradation of marine waters and sea ice melt does not result in significant outgassing of
534 CO_2 to the atmosphere via either the purely photochemical pathway or the combined
535 photochemical-biological pathway. Results presented here suggest that photodegradation of
536 under-ice waters is far more important for photobleaching (and changes in light penetration in
537 the euphotic zone) than it is for carbon cycling.
538
539 **5. Implications and Conclusions**
540 As the Arctic continues to warm and sea ice extent declines, the photoreactivity of DOM may
541 have important implications for primary productivity and the heat balance of the Arctic Ocean.
542 Thirty years ago much of the Arctic Ocean was covered with thick multi-year ice throughout the
543 summer [*Serreze et al*., 2007; *Kwok and Rothrock*, 2009], which limited the amount of UV and
544 visible light reaching under-ice waters. With decreasing sea ice extent and increases in thin first-
545 year ice and surface melt ponds, the surface layer of the Arctic Ocean is being exposed to more
546 solar radiation during the summer melt season. Several studies suggest that primary productivity
547 will increase in arctic waters owing to this decrease in sea ice extent [*Arrigo et al.,* 2008; *Arrigo*
548 *and van Dijken*, 2011] and increase in melt pond coverage [*Arrigo et al.,* 2012] and the
549 corresponding increase in PAR reaching ocean surface waters. However, continued ponding,
550 thinning, and ultimate loss of summer sea ice cover would also lead to a decrease in UV
551 absorption by surface CDOM with photodegradation. Combined with the unprecedented loss in
552 Arctic ozone in recent years [*Solomon et al.,* 2007; *Manney et al.*, 2011], this may result in
553 exposure of marine organisms to more harmful UV radiation and may in turn negatively impact
554 primary productivity. An additional complication is that the decrease in sea ice extent and

555 increase in open water during the summer months have been shown to coincide with an increase
556 in cloud coverage [*Wang and Key*, 2005; *Eastman and Warren*, 2010; *Palm et al*., 2010], which
557 limits the amount of shortwave radiation reaching the ocean surface. Models show that these
558 trends will likely continue in the future [*Vavrus et al.,* 2010] potentially counteracting the
559 increase in UV exposure owing to changes in sea ice, but also limiting the amount of available
560 PAR [*Belanger et al*., 2013]. This presents challenges for predicting future trends in the amount
561 of UV and visible radiation reaching surface waters and quantifying the overall impact that
562 CDOM photodegradation will have on primary production.
563
564 Warming temperatures in the Arctic are leading to permafrost thaw [*Romanovsky et al.*, 2010]
565 and increases in riverine discharge [*Peterson et al*., 2002], which in turn will likely lead to
566 increases in terrestrial DOM output to surface waters of the Arctic Ocean [*Frey and McClelland*,
567 2009]. Our results suggest that increasing terrestrial DOM supply will result in a measureable
568 increase in DOM photodegradation and loss of DOC, since significant changes in DOC were
569 observed in samples exhibiting greater contributions from humic-like terrestrially sourced
570 FDOM components. Increases in daily minimum flow rates, particularly in winter, have been
571 shown for arctic rivers [*Smith et al*., 2007], which could potentially increase the amount of
572 terrestrial DOM transported to surface waters of the Arctic Ocean [*Holmes et al*., 2008; *Stedmon*
573 *et al*., 2011]. Since this would occur when there is little light north of the Arctic Circle and the
574 Arctic Ocean is largely covered in sea ice, this DOM would initially be protected from
575 photodegradation and could be transported well into shelf seas and possibly the Arctic Ocean
576 basin interior. Furthermore, the spring freshet period has been shown to export a major fraction
577 of the annual DOM load of Arctic rivers and DOM exported during this period is relatively more

578 aromatic in character and more photolabile in comparison to other times of year [*Spencer et al.*,
579 2008; *Holmes et al.*, 2012; *Mann et al.*, 2012]. This major pulse of photoreactive DOM enters the
580 Arctic Ocean at the onset of spring and thus with the decrease in sea ice extent and increase in
581 melt ponding during the following spring and summer, our results suggest that this DOM would
582 be poised for significant photodegradation during the subsequent melt season. This combined
583 with increased DOM from under-ice blooms and subsequent photodegradation could alter CO_2
584 saturation in surface waters.
585
586 By absorbing sunlight and subsequently re-emitting it as heat, CDOM also contributes to the
587 heating of surface waters [*Kirk,* 1988]. With increasing sea ice melt, more light may be
588 transmitted through sea ice and absorbed and emitted as heat by the existing CDOM below. This
589 increase in heat absorption by the under-ice water column could increase local sea surface
590 temperatures and potentially lead to further sea ice melt from below, thus initiating a positive
591 feedback to sea ice melt [*Hill*, 2008]. A future increase in CDOM supply, particularly from
592 riverine sources, would considerably increase CDOM absorption and it is likely that
593 photodegradation will substantially decrease the light absorption of this additional riverine
594 CDOM. At present, the combined effect of increases in CDOM additions from *in situ*
595 production and riverine sources as well as increasing CDOM photobleaching as ice cover
596 recedes upon ocean surface heating remain unclear.
597
598 In conclusion, our observed reductions in CDOM absorbance at shorter wavelengths suggest that
599 the beneficial UV protection currently received by marine organisms may significantly reduce
600 with sea ice melt ponding and overall declines of sea ice cover. However, some of these CDOM

losses may be balanced by increasing CDOM inputs from increased primary production and terrestrial carbon export. We additionally show that under current conditions, photodegradation of CDOM in under-ice waters is not a significant source of CO_2, and it is unclear whether the potential for surface ocean heating is compromised with irradiation. However, as arctic temperatures warm and summer sea ice continues to disappear, continued examination of the resulting enhanced photodegradation processes and their impacts on the interplay between primary production, carbon biogeochemistry, and surface ocean heating will be vital.

Acknowledgements

All data in this study are currently available either in tables within this manuscript or upon request from the corresponding author (kfrey@clarku.edu), and will additionally be available at the ACADIS Arctic Data Repository (http://www.aoncadis.org). This research was part of the NASA Impacts of Climate change on the Ecosystems and Chemistry of the Arctic Pacific Environment (ICESCAPE) project with support from the NASA Cryospheric Sciences Program (Grant #NNX10AH71G to K. Frey) and the NASA Ocean Biology and Biogeochemistry Program. The field component of this research would not have been possible without the tremendous support from the commanding officer, marine science technicians, crew, and officers of USCGC *Healy* on the HLY1101 mission to the Chukchi and Beaufort seas in June-July 2011. We thank Dr. Leanne Powers for assistance generating modelled solar irradiance data. Additional funding was provided by NSF DEB-1146161 to A. Stubbins and NSF ANT-1203885/PLR-1500169 to R. Spencer.

References

Amon, R.M.W. (2003) The role of dissolved organic matter for the organic carbon cycle in the Arctic Ocean, in The Organic Carbon Cycle in the Arctic Ocean, edited by R. Stein R. MacDonald, pp. 83-99, Springer, Berlin.

Arrigo, K. R. and G. L. van Dijken (2011), Secular trends in Arctic Ocean net primary production, Journal of Geophysical Research, 116, C09011, doi:10.1029/2011JC007151.

Arrigo, K. R., G. van Dijken and S. Pabi (2008), Impact of a shrinking Arctic ice cover on marine primary production, Geophysical Research Letters, 35, L19603, doi:10.1029/2008GL035028.

Arrigo, K. R. et al. (2012), Massive phytoplankton blooms under Arctic sea ice, Science, 336, 1407-1408.

Baker, A., and R. G. M. Spencer, (2004), Characterization of dissolved organic matter from source to sea using fluorescence and absorbance spectroscopy, Science of the Total Environment 333, 217-232.

Belanger, S., H. Xie, N. Krotkov, and P. Larouche (2006) Photomineralization of terrigenous dissolved organic matter in Arctic coastal waters from 1979 to2003: Interannual variability and implications of climate change, Global Biogeochemical Cycles, 20, GB4005, doi:10.1029/2006GB002708.

Belanger, S., M. Babin and J.-E. Tremblay (2013), Increasing cloudiness in Arctic damps the increase in phytoplankton primary production due to sea ice receding, Biogeosciences, 10, 4087–4101, doi:10.5194/bg-10-4087-2013.

Benner, R., and B. Biddanda (1998), Photochemical transformations of surface and deep marine dissolved organic matter: Effects on bacterial growth, Limnol. Oceanogr., 43(6), 1373-1378.

Bittar, T. B., A. A. H. Vieira, A. Stubbins and K. Mopper, (2015), Competition between photochemical and biological degradation of dissolved organic matter from the cyanobacteria Microcystis aeruginosa, Limnology and Oceanography, 60(4), 1172-1194.

Brown, M. (1977), Transmission spectroscopy examinations of natural waters, Estuar. Coast. Mar. Sci., 5, 309-317, doi: 10.1016/0302-3524(77)90058-5.

Blough, N.V., and R. Del Vecchio (2002), Chromophoic DOM in the coastal environment, in Biogeochemistry of Marine Dissolved Organic Matter, edited by D.A. Hansell and C.A. Carlson, pp. 509-546, Elsevier, San Diego, Calif.

668 Carlson (2002), Production and Removal Processes, in Biogeochemistry of Marine Dissolved
669 Organic Matter, edited by D.A. Hansell and C.A. Carlson, pp. 91-151, Elsevier, San Diego,
670 Calif.
671
672 Coble, P.G. (1996). Characterization of marine and terrestrial DOM in seawater using excitation-
673 emission matrix spectroscopy, Mar. Chem., 51, 325-346.
674
675 Coble, P.G. (2007), Marine Optical Biogeochemistry: The Chemistry of Ocean Color, Chem.
676 Rev., 107, 402-418.
677
678 Comiso, J. C., C. L. Parkinson, R. Gersten, and L. Stock (2008), Accelerated decline in the
679 Arctic sea ice cover, Geophys. Res. Lett., 35, L01703, doi:10.1029/2007GL031972.
680
681 Comiso, J. C. (2012), Large decadal decline of the Arctic multiyear ice cover, J. Clim., 25(4),
682 1176–1193, doi:10.1175/JCLI-D-11-00113.1.
683
684 Del Vecchio, R., and N. V. Blough (2004), Spatial and seasonal distribution of chromophoric
685 dissolved organic matter and dissolved organic carbon in the Middle Atlantic Bight, Mar. Chem.,
686 89(1–4), 169–187, doi:10.1016/j.marchem.2004.02.027.
687
688 Dittmar, T., and G. Kattner (2003), The biogeochemistry of the river and shelf ecosystem of the
689 Arctic Ocean: a review, Marine Chemistry, 83, 103-120, doi:10.1016/S0304-4203(03)00105-1.
690
691 Eastman, R. and S. G. Warren (2010) Arctic Cloud Changes from Surface and Satellite
692 Observations, Journal of Climate, 23, 4233-4242,doi:10.1175/2010JCLI3544.1.
693
694 Fellman, J.R., E. Hood, R.G.M Spencer, (2010), Fluorescence spectroscopy opens new windows
695 into dissolved organic matter dynamics in freshwater ecosystems: A review, Limnology and
696 Oceanography, 55, 2452-2462.
697
698 Ferrari, G. M., M. D. Dowell, S. Grossi, and C. Targa (1996), Relationship between the optical
699 properties of chromophoric dissolved organic matter and total concentration of dissolved organic
700 carbon in the southern Baltic Sea region, Mar. Chem., 55(3–4), 299–316.
701
702 Fetterer, F. and N. Untersteiner (1998), Observations of melt ponds on Arctic sea ice, Journal of
703 Geophysical Research, 103(C11), 24, 821–24,835.
704
705 Fichot, C. G. and R. Benner (2011), A novel method to estimate DOC concentrations from
706 CDOM absorption coefficients in coastal waters, Geophysical Research Letters, 38, L03610,
707 doi:10.1029/2010GL046152.
708
709 Frey, K. E. and J. W. McClelland (2009), Impacts of permafrost degradation on arctic river
710 biogeochemistry, Hydrological Processes, 23, 169-182, doi:10.1002/hyp.7196.
711
712 Frey, K. E., D. K. Perovich, and B. Light (2011), The spatial distribution of solar radiation under
713 a melting Arctic sea ice cover, Geophys. Res. Lett., 38, L22501, doi:10.1029/2011GL049421.

Graeber, D., J. Gelbrecht, M. Pusch, C. Anlanger, and D. von Schiller (2012), Agriculture has changed the amount and composition of dissolved organic matter in Central European headwater streams, Science of The Total Environment, 438, 435-446.

Granskog, M. A., R. W. Macdonald, C. J. Mundy and D. G. Barber (2007) Distribution, characteristics and potential impacts of chromophoric dissolved organic matter (CDOM) in Hudson Strait and Hudson Bay, Canada, Continental Shelf Research, 27, 2032-2050. doi:10.1016/j.csr.2007.05.001.

Green, S. A., and N. V. Blough (1994), Optical absorption and fluorescence properties of chromophoric dissolved organic matter in natural waters, Limnol. Oceanogr., 39, 1903-1916.

Gueguen, C., L. Guo, and N. Tanaka (2005), Ditributions and characteristics of colored dissolved organic matter in the Western Arctic Ocean, Continental Shelf Research, 25, 1195-1207, doi:10.1016/j.csr.2005.01.005.

Gueguen, C., L., Guo, M. Yamamoto-Kawai, and N. Tanaka (2007), Colored dissolved organic matter dynamics across the shelf-basin interface in the western Arctic Ocean, Journal of Geophysical Research, 112, C05038, doi:10.1029/2006JC003584.

Helms, J. R., A. Stubbins, J. D. Ritchie, E. C. Minor, D. J. Kieber, and K. Mopper (2008), Absorption spectral slopes, and slope ratios as indicators of molecular weight, source, and photobleaching of chromophoric dissolved organic matter, Limnol. Oceanogr., 53, 955-969.

Helms, J.R., J. Mao, A. Stubbins, K. Schmidt-Rohr, R.G.M. Spencer, P.J. Hernes and K. Mopper (2014), Loss of optical and molecular indicators of terrigenous dissolved organic matter during long-term photobleaching. Aquatic Sciences., 76(3), 353-373.

Hill, V. J. (2008), Impacts of chromophoric dissolved organic material on surface ocean heating in the Chukchi Sea, Journal of Geophysical Research, 113, C07024, doi:10.1029/2007JC004119.

Holmes, R. M., J. W. McClelland, P. A. Raymond, B. B. Frazer, B. J. Peterson and M. Stieglitz (2008), Lability of DOC transported by Alaskan rivers to the Arctic Ocean, Geophysical Research Letters, 35, L03402, doi:10.1029/2007GL032837.

Holmes, R. M., J. W. McClelland, B. J. Peterson, S. E. Tank, E. Bulygina, T. I. Eglinton, V. V. Gordeev, T. Y. Gurtovaya, P. A. Raymond, D. J. Repeta, R. Staples, R. G. Striegl, A. V. Zhulidov, and S. A. Zimov (2012), Seasonal and annual fluxes of nutrients and organic matter from large rivers to the Arctic Ocean and surrounding seas, Estuaries and Coasts 35, 369-382, doi: 10.1007/s12237-011-9386-6.

Jørgensen, L., C. A. Stedmon, T. Kragh, S. Markager, M. Middelboe, and M. Søndergaard (2011), Global trends in the fluorescence characteristics and distribution of marine dissolved organic matter, Mar. Chem., 126, 139-148, doi:10.1016/j.marchem.2011.05.002.

760 Kirk, J.T.O. (1988), Solar heating of water bodies as influenced by their inherent optical
761 properties, Journal of Geophysical Research, 93, D9, 10897–10908.
762
763 Kirk, J. T. O. (1994), Light and Photosynthesis in Aquatic Ecosystems, Cambridge Univ. Press,
764 Cambridge, U.K.
765
766 Kitidis, V., A. P. Stubbins, G. Uher, R. C. U. Goddard, C. S. Law and E. M. S. Woodward
767 (2006),Variability of chromophoric organic matter in surface waters of the Atlantic Ocean, Deep
768 Sea Research Part II: Topical Studies in Oceanography, 53(14), 1666-1684.
769
770 Kowalczuk, P., M. J. Durako, H. Young, A. E. Kahn, W. J. Cooper, and M. Gonsior (2009),
771 Characterization of dissolved organic matter fluorescence in the South Atlantic Bight with use of
772 PARAFAC model: Interannual variability, Marine Chemistry, 113, 182-196.
773
774 Kwok, R., and D. A. Rothrock (2009), Decline in Arctic sea ice thickness from submarine and
775 ICESat records: 1958-2008, Geophys. Res. Lett., 36, L15501, doi:10.1029/2009GL039035.
776
777 Lawaetz, A.J., and C.A. Stedmon (2009), Fluorescence intensity calibration using the Raman
778 scatter peak of water, Appl. Spectrosc., 63 (8), 936-940.
779
780 Light, B., T. C. Grenfell, and D. K. Perovich (2008), Transmissionand absorption of solar
781 radiationby Arctic sea ice during the melt season, J. Geophys. Res., 113, C03023,
782 doi:10.1029/206JC003977.
783
784 Mann, P. J. (2010) Ammonium Photoproduction and CDOM Biogeochemistry in Marine
785 Systems. PhD thesis. Newcastle University, UK.
786
787 Mann, P.J., A. Davidova, N. Zimov, R.G.M. Spencer, S. Davydov, E. Bulygina, S. Zimov, R.M.
788 Holmes (2012), Controls on the composition and lability of dissolved organic matter in Siberia's
789 Kolyma River Basin, J. Geophys. Res. 117, G01028, doi:10.1029/2011JG001798.
790
791 Manney, G. L. et al. (2011), Unprecedented Arctic ozone loss in 2011, Nature, 478, 469-475,
792 doi:10.1038/nature10556.
793
794 Markus, T., J. C. Stroeve, and J. Miller (2009), Recent changes in Arctic sea ice melt onset,
795 freezeup , and melt season length, J. Geophys. Res., 114, C12024, doi:10:1029/2009JC005436.
796
797 Maslanik, J.A., C. Fowler, J. Stroeve, S. drobot, J. Zwally, D. Yi, and W. Emery (2007), A
798 younger, thinner Arctic ice cover: Increased potential for rapid, extensive sea-ice loss, Geophys.
799 Res. Lett., 34, L24501, doi:10:1029/2007GL032043.
800
801 Maslanik, J., J. Stroeve, C. Fowler, and W. Emery (2011), Distribution and trends in Arctic sea
802 ice age through spring 2011, Geophys. Res. Lett., 38, L13502, doi:10.1029/2011GL047735.
803

804 Matsuoka, A., Y. Huot, K. Shimada, S. Saitoh and M. Babin (2007), Bio-optical characteristics
805 of the western Arctic Ocean: implications for ocean color algorithms, Can. J. Remote Sensing,
806 33(6), 503-518, doi
807
808 Matsuoka, A., V. Hill, Y. Huot, M. Babin and A. Bricaud (2011), Seasonal variability in the light
809 absorption properties of western Arctic waters: Parameterization of the individual components of
810 absorption for ocean color applications, Journal of Geophysical Research, 116, C02007,
811 doi:10.1029/2009JC005594.
812
813 Mopper, K., D. Kieber, and A. Stubbins (2015), Marine Photochemistry: Processes and Impacts,
814 in Biogeochemistry of Marine Dissolved Organic Matter, 2nd Edition, edited by D.A. Hansell
815 and C.A. Carlson, Elsevier, San Diego, Calif.
816
817 Moran, M. A., and R. G. Zepp (1997), Role of Photoreactions in the Formation of Biologically
818 Labile Compounds from Dissolved Organic Matter, Limnology and Oceanography, 42, 1307-
819 1316.
820
821 Moran, M. A., W. M. Sheldon and R. G. Zepp (2000), Carbon loss and optical property changes
822 during long-term photochemical and biological degradation of estuarine dissolved organic
823 matter, Limnol. Oceanogr., 45(6), 2000, 1254-1264.
824
825 Murphy, K.R., C.A. Stedmon, T.D. Waite, and G.M. Ruiz (2008), Distinguishing between
826 terrestrial and autochthonous organic matter sources in marine environments using fluorescence
827 spectroscopy, Marine Chemistry, 108, 40-58.
828
829 Murphy, K.R., K.D. Butler, R.G.M. Spencer, C.A. Stedmon, J.R. Boehme, G.R. Aiken (2010),
830 Measurement of dissolved organic matter fluorescence in aquatic environments: An
831 interlaboratory comparison, Environmental, Science and Technology 44, 9405-9412.
832
833 Murphy, K.R., A. Hambly, S. Singh, R.K. Henderson, A. Baker, R. Stuetz, and S.J. Khan (2011),
834 Organic matter fluorescence in municipal water recycling schemes: toward a unified PARAFAC
835 model. Environ. Sci. Technol., 45, 2909-2916.
836
837 Murphy, K.R., R. Bro, and C.A. Stedmon (2014a), Chemometric analysis of organic matter
838 fluorescence. in: Coble, P., Baker, A., Lead, J., Reynolds, D., Spencer, R. (Eds.). Aquatic
839 organic matter fluorescence. Cambridge University Press, New York.
840
841 Murphy K.R., C.A. Stedmon, P. Wenig R. Bro (2014b), OpenFluor - A spectral database of auto-
842 fluorescence by organic compounds in the environment. Anal. Methods, 6, 658-661.
843 doi:10.1039/C3AY41935E
844
845 Nelson, N.B., and D.A. Siegel (2002) Chromophoic DOM in the open ocean, in Biogeochemistry
846 of Marine Dissolved Organic Matter, edited by D.A. Hansell and C.A. Carlson, pp. 547-578,
847 Elsevier, San Diego, Calif.
848

849 Nicolaus, M., C. Katlein, J. Maslanik, and S. Hendricks (2012), Changes in Arctic sea ice result
850 in increasing light transmittance and absorption, Geophys. Res. Lett., 39, L24501,
851 doi:10.1029/2012GL053738.
852
853 Norman, L., D. N. Thomas, C. A. Stedmon, M. A. Granskog, S. Papadimitriou, R. Krapp, K. M.
854 Meiners, D. Lannuzel, P. van der Merwe and G. S. Dieckmann (2011), The characteristics of
855 chromophoric dissolved organic matter (CDOM) in Antarctic sea ice, Deep-Sea Res. II, 58,
856 1075-1091, doi:10.1016/j.dsr2.2010.10.030.
857
858 Obernosterer, I., B. Reitner and G. Herndl (1999), Contrasting effects of solar radiation on
859 dissolved organic matter and its bioavailability to marine bacterioplankton, Limnol. Oceanogr.,
860 44(7), 1645–1654.
861
862 Obernosterer, I., R. Sempere and G. J. Herndl (2001) Ultraviolet radiation induces reversal of the
863 bioavailability of DOM to marine bacterioplankton. Aquatic Microbial Ecology, 24(1), 61-68.
864
865 Opsahl, S., R. Benner, and R. M. Amon (1999), Major flux of terrigenous dissolved organic
866 matter through the Arctic Ocean, Limnol. Oceanogr., 44,(8) 2017-2023,
867 doi:10.4319/lo.1999.44.8.2017.
868
869 Osburn, C.L., Morris, D.P., Thorn, K.A., Moeller, R.E., 2001. Chemical and optical changes in
870 freshwater dissolved organic matter exposed to solar radiation. Biogeochemistry, 54(3): 251-278.
871
872 Osburn, C. L., L. Retamal and W. F. Vincent (2009), Photoreactivity of chromophoric dissolved
873 organic matter transported by the Mackenzie River to the Beaufort Sea, Marine Chemistry, 115,
874 10-20, doi:10.1016/j.marchem.2009.05.003.
875
876 Palm, S. P., S. T. Strey, J. Spinhirne and T. Markus (2010), Influence of Arctic sea ice extent on
877 polar cloud fraction and vertical structure and implications for regional climate, Journal of
878 Geophysical Research, 115, D21209, doi:10.1029/2010JD013900.
879
880 Pegau,W. S. (2002), Inherent optical properties of the central Arctic surface waters, Journal of
881 Geophysical Research, 107(C10), 8035, doi:10.1029/2000JC000382.
882
883 Perovich, D. K., B. Light, H. Eicken, K. F. Jones, K. Runciman, and S. V. Nghiem (2007),
884 Increasing solar heating of the Arctic Ocean and adjacent seas, 1979-2005: Attribution and role
885 in the ice-albedo feedback, Geophysical Research Letters, 34, L19505,
886 doi:10.1029/2007GL031480.
887
888 Perovich, D., W. Meier, M. Tschudi, S. Gerland, J. Richter-Menge (2012), Sea Ice [In Arctic
889 Report Card 2012], http://www.arctic.noaa.gov/reportcard.
890
891 Peterson, B. J., R. M. Holmes, J. W. McClelland, C. J. Vorosmarty, I. A. Shiklomonov, R. B.
892 Lammers, and S. Rahmstorf (2002), Increasing river discharge to the Arctic Ocean, Science, 298,
893 2171-2173.
894

Powers, L. C., and W. L. Miller (2015), Photochemical production of CO and CO_2 in the Northern Gulf of Mexico: Estimates and challenges for quantifying the impact of photochemistry on carbon cycles, Marine Chemistry, 171: 21-35.

Raymond, P.A. and R. G.M. Spencer, (2105), Riverine DOM, in Biogeochemistry of Marine Dissolved Organic Matter (Second Edition), edited by Dennis A. Hansell Craig A. Carlson, Academic Press, Boston, pp. 509-533, ISBN 9780124059405, http://dx.doi.org/10.1016/B978-0-12-405940-5.00011-X.

Retamal, L., W. F. Vincent, C. Martineau and C. L. Osburn (2007), Comparison of the optical properties of dissolved organic matter in two river-influenced coastal regions of the Canadian Arctic, Estuarine, Coastal and Shelf Science, 72, 261-272, doi:10.1016/j.ecss.2006.10.022.

Retamal, L., Bonilla, S. et al. (2008), Optical gradients and phytoplankton production in the Mackenzie River and the coastal Beaufort Sea, Polar Biology, 31(3), 363-379.

Romanovsky, V. E., S. L. Smith and H. H. Christiansen (2010), Permafrost Thermal State in the Polar Northern Hemisphere during the International Polar Year 2007–2009: a Synthesis, Permafrost and Periglac. Process., 21, 106–116, doi:10.1002/ppp.689.

Ruggaber, A., R. Dlugi and T. Nakajima (1994), Modelling radiation quantities and photolysis frequencies in the troposphere, Journal of Atmospheric Chemistry, 18(2), 171-210.

Schröder, D., D. L. Feltham, D. Flocco and M. Tsamados (2014), September Arctic sea-ice minimum predicted by spring melt-pond fraction, Nature Climate Change, 4, 353-357, doi: 10.1038/nclimate2203.

Scully, N., and M. W. L. Miller (2000), Spatial and temporal dynamics of colored dissolved organic matter in the north water polynya, Geophys. Res. Lett., 27, 1009–1011.

Seredynska-Sobecka, B., C.A. Stedmon, R. Boe-Hansen, C.K. Waul, and E. Arvin (2011), Monitoring organic loading to swimming pools by fluorescence excitation-emission matrix with parallel factor analysis (PARAFAC), Water Research, 45 (6), 2306-2314.

Serreze, M.C., M. M. Holland, and J. Stroeve (2007), Perspectives on the Arctic's shrinking sea ice cover, Science, 315, 133-1536, doi:10:1126/science.1139426.

Shutova, Y., A. Baker, J. Bridgeman and R.K. Henderson (2014), Spectroscopic characterisation of dissolved organic matter changes in drinking water treatment: from PARAFAC analysis to online monitoring wavelengths, Water Research, 54, 159-169.

Smith, L. C., T. M. Pavelsky, G. M. MacDonald, A. I. Shiklomanov and R. B. Lammers (2007), Rising minimum daily flows in northern Eurasian rivers: A growing influence of groundwater in the high-latitude hydrologic cycle, Journal of Geophysical Research, 112, G04S47, doi:10.1029/2006JG000327.

941
942 Solomon, S., R. W. Portmann, and D. W. J. Thomas (2007), Contrasts between Antarctic and
943 Arctic ozone depletion, Proceedings of the National Academy of Sciences, 104(2), 445-449.
944
945 Spencer, R.G.M., G.R. Aiken, K.P. Wickland, R.G. Striegl, P.J. Hernes (2008), Seasonal and
946 spatial variability in dissolved organic matter quantity and composition from the Yukon River
947 Basin, Alaska, Global Biogeochemical Cycles, 22, GB4002, doi:10.1029/ 2008GB003231.
948
949 Spencer, R. G. M., et al. (2009), Photochemical degradation of dissolved organic matter and
950 dissolved lignin phenols from the Congo River, J. Geophys. Res., 114, G03010,
951 doi:10.1029/2009JG000968.
952
953 Spencer, R.G.M., K.D., Butler and G.R., Aiken (2012)' Dissolved organic carbon and
954 chromophoric dissolved organic matter properties of rivers in the U.S.A., Journal of Geophysical
955 Research – Biogeosciences, 117, G03001, doi:10.1029/2011JG001928.
956
957 Stedmon, C.A., and S. Markager (2001), The optics of chromophoric dissolved organic matter
958 (CDOM) in the Greenland Sea: An algorithm for differentiation between marine and terrestrially
959 derived organic matter, Limnol. Oceanogr., 46, 2087–2093.
960
961 Stedmon , C. A., S. Markager, R. Bro (2003), Tracing dissolved organic matter in aquatic
962 environments using a new approach to fluorescence spectroscopy, Mar. Chem., 82, 239-254,
963 doi:10.1016/S0304-4203(03)00072-0.
964
965 Stedmon, C.A. and S. Markager (2005a), Resolving the variability of dissolved organic matter
966 fluorescence in a temperate estuary and its catchment using PARAFAC analysis, Limnology and
967 Oceanography, 50, 686–697.
968
969 Stedmon, C.A. and S. Markager (2005b), Tracing the production and degradation of
970 autochthonous fractions of dissolved organic matter using fluorescence analysis, Limnology and
971 Oceanography, 50 (5), 1415–1426.
972
973 Stedmon, C.A., S. Markager, L. Tranvik, L. Kronberg, T. Slätis and W. Martinsen (2007a),
974 Photochemical production of ammonium and transformation of dissolved organic matter in the
975 Baltic Sea, Mar. Chem., 104, 227-240, doi:10.1016/j.marchem.2006.11.005.
976
977 Stedmon, C.A., D.N. Thomas, M. Granskog, H. Kaartokallio, S. Papadimitriou, and H. Kuosa
978 (2007b), Characteristics of Dissolved Organic Matter in Baltic Coastal Sea Ice: Allochthonous or
979 Autochthonous Origins?, Environ. Sci. Technol., 41, 7273-7279.
980
981 Stedmon, C.A., and R. Bro (2008), Characterizing dissolved organic matter fluorescence with
982 parallel factor analysis: A tutorial, Limnol. Oceanogr. Methods, 6, 572-579.
983
984 Stedmon, C.A., R.M.W. Amon, A.J. Rinehart, S.A. Walker (2011), The supply and
985 characteristics of colored dissolved organic matter (CDOM) in the Arctic Ocean: Pan Arctic
986 trends and differences, Mar. Chem., 124, 108-118, doi:10.1016/j.marchem.2010.12.007.

Stroeve, J., M. M. Holland, W. Meier, T. Scambos, and M. Serreze (2007), Arctic sea ice decline: Faster than forecast, Geophys. Res. Lett., 34, L09501, doi:10.1029/2007GL029703.

Stubbins, A., V. Hubbard, G. Uher, C. S. Law, R. C. Upstill-Goddard, G. R. Aiken, and K. Mopper (2008), Relating Carbon Monoxide Photoproduction to Dissolved Organic Matter Functionality, Environ. Sci. Technol. , 42, 3271-3276, doi.

Stubbins, A., R. G. M. Spencer, H. Chen, P. G. Hatcher, K. Mopper, P. J. Hernes, V. L. Mwamba, A. M. Mangangu, J. N. Wabakanghanzi, and J. Six (2010), Illuminated darkness: molecular signatures of Congo River dissolved organic matter and its photochemical alteration as revealed by ultrahigh precision mass spectrometry, Limnol. Oceanogr., 55, 1467–1477, doi:10.4319/lo.2010.55.4.1467.

Stubbins, A., and T. Dittmar (2012), Low volume quantification of dissolved organic carbon and dissolved nitrogen, Limnol. Oceanogr. Methods. 10, 347-352, doi:10.4319/lom.2012.10.347.

Stubbins, A., J.-F. Lapierre, M. Berggren, Y. Prairie, T. Dittmar, and P. del Giorgio, (2014), What's in an EEM? Molecular signatures associated with dissolved organic fluorescence in boreal Canada, Environmental Science and Technology, doi: 10.1021/es502086e.

Tanaka, K., K. Kuma, K. Hamasaki, and Y. Yamashita (2014) Accumulation of humic-like fluorescent dissolved organic matter in the Japan Sea, Scientific Reports, 4, 5292.

Tranvik, L. and S. Kokalj (1998) Decreased biodegrability of algal DOC due to interactive effects of UV radiation and humic matter, Aquat. Microb. Ecol., 14, 301-307.

Tranvik, L. J., H. Olofsson and S. Bertilsson (1999) Photochemical Effects on Bacterial Degradation of Dissolved Organic Matter in Lake Water, in Microbial Biosystems: New Frontiers Proceedings of the 8th International Symposium on Microbial Ecology edited by C. R. Bell, M. Brylinsky and P. Johnson-Green, Atlantic Canada Society for Microbial Ecology, Halifax, Canada.

Tranvik, L. J., and S. Bertilsson (2001), Contrasting effects of solar UV radiation on dissolved organic sources for bacterial growth, Ecol. Lett., 4. doi: 10.1046/j.1461-0248.2001.00245.x

Vahatalo, A. V. and R. G. Wetzel (2004) Photochemical and microbial decomposition of chromophoric dissolved organic matter during long (months–years) exposures, Marine Chemistry, 89, 313– 326, doi:10.1016/j.marchem.2004.03.010.

Vavrus, S., M. M. Holland, and D. A. Bailey (2010), Changes in Arctic clouds during intervals of rapid sea ice loss, Climate Dynamics, 36, 1475–1489, doi:10.1007/s00382-010-0816-0, 2010.

Walker, S. A., R. M. W. Amon, C. Stedmon, S. Duan, and P. Louchouarn (2009), The use of PARAFAC modeling to trace terrestrial dissolved organic matter and fingerprint water masses in

coastal Canadian Arctic surface waters, J. Geophys. Res., 114, G00F06, doi:10.1029/2009JG000990.

Wang, X. and J. R. Key (2005), Arctic Surface, Cloud, and Radiation Properties Based on the AVHRR Polar Pathfinder Dataset. Part II: Recent Trends, Journal of Climate, 18, 2575-2593.

Wang, M. and J. E. Overland (2009), A sea ice free summer Arctic within 30 years?, Geophys. Res. Lett., 36, L07502, doi:10.1029/2009GL037820.

Williamson, C.E., Neale, P.J et al. (2001), Beneficial and detrimental effects of UV on aquatic organisms: Implications of spectral variation, Ecological Applications, 11(6), 1843–1857.

Yamashita, Y., R. M. Cory, J. Nishioka, K. Kuma, E. Tanoue, R. Jaffé (2010a), Fluorescence characteristics of dissolved organic matter in the deep waters of the Okhotsk Sea and the northwestern North Pacific Ocean, Deep-sea Research II, 57, 1478–1485.

Yamashita, Y., L.J. Scinto, N. Maie, and R. Jaffe (2010b), Dissolved Organic Matter Characteristics Across a Subtropical Wetland Landscape: Application of Optical Properties in the Assessment of Environmental Dynamics, Ecosystems, 13, 1006-1019.

Yamashita, Y., B.D. Kloeppel, J. Knoepp, G.L. Zausen, and R. Jaffe (2011), Effects of Watershed History on Dissolved Organic Matter Characteristics in Headwater Streams, Ecosystems, 14, 1110-1122.

Yamashita, Y., J.N. Boyer, and R. Jaffe (2013), Evaluating the distribution of terrestrial dissolved organic matter in a complex coastal ecosystem using fluorescence spectroscopy, Continental Shelf Research, 66, 136-144.

Table 1. Initial, final and percent remaining after 72 hour irradiation experiments for a_{254} and DOC for all experiments. Bold numbers indicate statistically significant changes ($p < 0.05$). *NA* indicates that the value is unavailable owing to sample loss.

Sample Name	Collection Date	Salinity		a_{254} (m^{-1})	DOC (μM)
ICM_1	7/4/2011	17.4	Initial	1.41 ± 0.03	67.8 ± 0.8
			Final	0.66 ± 0.02	65.8 ± 1.2
			% Remaining	**47.1**	97.0
ICM_2	7/5/2011	30.7	Initial	1.55 ± 0.01	71.9 ± 2.8
			Final	0.72 ± 0.02	68.7 ± 1.2
			% Remaining	**46.5**	95.6
ICM_3	7/6/2011	29.7	Initial	1.37 ± 0.04	61.1 ± 2.5
			Final	0.62 ± 0.01	60.6 ± 0.4
			% Remaining	**44.8**	99.1
ICM_4	7/10/2011	22.4	Initial	1.36 ± 0.02	53.6 ± 3.9
			Final	0.63 ± 0.01	53.7 ± 2.4
			% Remaining	**46.5**	100.2
ICM_5	7/13/2011	24.9	Initial	2.17 ± 0.01	71.1 ± 0.1
			Final	0.98 ± 0.03	68.0 ± 1.3
			% Remaining	**44.9**	95.6
ICM_6	07/19/11	20.8	Initial	2.01 ± 0.03	69.4 ± 0.6
			Final	0.98 ± 0.02	67.0 ± 0.8
			% Remaining	**48.7**	**96.6**
IFM_1	7/3/2011	31.7	Initial	1.49 ± 0.04	
			Final	0.77 ± 0.04	*NA*
			% Remaining	**51.8**	
IFM_2	7/9/2011	31.1	Initial	1.89 ± 0.01	71.2 ± 0.9
			Final	0.83 ± 0.02	71.9 ± 1.1
			% Remaining	**44.0**	100.9
IFT_1	07/21/11	28.0	Initial	5.79 ± 0.03	105.4 ± 1.4
			Final	2.17 ± 0.05	97.1 ± 2.5
			% Remaining	**37.4**	**92.1**
IFT_2	07/20/11	24.4	Initial	3.12 ± 0.00	80.5 ± 1.2
			Final	1.48 ± 0.06	74.7 ± 0.6
			% Remaining	**47.4**	**92.8**

Formatted: Numbering: Continuous

Table 2. Average initial and final values for the 72 hour irradiation experiments for a_{254}, a_{365} and a_{440} for ice-covered marine (ICM), ice-free marine (IFM), and ice-free terrestrial (IFT) samples.

		a_{254} (m^{-1})	a_{365} (m^{-1})	a_{440} (m^{-1})
ICM_{mean}	Initial	1.62 ± 0.32	0.14 ± 0.02	0.04 ± 0.01
	Final	0.76 ± 0.16	0.06 ± 0.01	0.02 ±0.01
IFM_{mean}	Initial	1.69 ± 0.22	0.17 ± 0.03	0.06 ± 0.01
	Final	0.80 ± 0.05	0.08 ± 0.02	0.04 ± 0.01
IFT_{mean}	Initial	4.46 ± 1.46	0.50 ± 0.29	0.13 ± 0.08
	Final	1.82 ± 0.38	0.18 ± 0.08	0.05 ± 0.03

Table 3. Three parameter exponential decay models for a_{254} vs. cumulative UV light absorbed for all experiments.

	ICM_1	ICM_2	ICM_3	ICM_4	ICM_5	ICM_6	IFM_1	IFM_2	IFT_1	IFT_2
z_0	0.78	0.90	0.80	0.80	1.28	1.08	0.73	1.17	4.21	1.77
K	1.64	2.25	1.94	1.74	1.41	1.54	1.96	0.82	0.25	0.81
C_∞	0.63	0.71	0.59	0.57	0.89	0.91	0.76	0.68	1.63	1.36
$C(0)$	1.42	1.60	1.39	1.36	2.17	1.99	1.49	1.86	5.84	3.13
R^2	0.96	0.98	0.97	0.97	0.96	0.96	0.96	0.94	0.98	0.98

Table 4. Initial, final and percent remaining after 72 hour irradiation experiments for the spectral slope parameters $S_{275–295}$, $S_{350–400}$, and S_R for all experiments. Bold numbers indicate statistically significant changes ($p < 0.05$).

		ICM_1	**ICM_2**	**ICM_3**	**ICM_4**	**ICM_5**	**ICM_6**	**IFM_1**	**IFM_2**	**IFT_1**	**IFT_2**
	Initial	0.0241	0.0266	0.0264	0.0299	0.0311	0.0337	0.0255	0.0260	0.0203	0.0284
$S_{275–295}$	Final	0.0233	0.0238	0.0238	0.0257	0.0259	0.0255	0.0197	0.0249	0.0202	0.0242
	Difference	**-0.0008**	**-0.0028**	**-0.0026**	**-0.0043**	**-0.0052**	**-0.0081**	**-0.0057**	**-0.0011**	-0.0001	**-0.0041**
	Initial	0.0180	0.0170	0.0185	0.0217	0.0161	0.0197	0.0148	0.0170	0.0184	0.0202
$S_{350–400}$	Final	0.0136	0.0158	0.0116	0.0139	0.0181	0.0188	0.0121	0.0109	0.0171	0.0198
	Difference	**-0.0044**	**-0.0012**	**-0.0069**	**-0.0078**	0.0021	**-0.0009**	**-0.0026**	**-0.0060**	**-0.0013**	**-0.0004**
	Initial	1.3371	1.5692	1.4257	1.3830	1.9370	1.7120	1.7253	1.5275	1.1029	1.4046
S_R	Final	1.7154	1.5036	2.0480	1.8492	1.4288	1.3581	1.6264	2.2728	1.1793	1.2241
	Difference	**0.3783**	-0.0656	**0.6223**	**0.4662**	-0.5081	**-0.3539**	-0.0989	**0.7452**	**0.0764**	-0.1805

Table 5. Spectral characteristics of the six components identified by PARAFAC compared to previously identified components. Secondary maxima are shown in parentheses. Component matches (>0.95 tucker congruent coefficient) identified using the OpenFluor database (http://www.openfluor.org, *Murphy et al.* [2014b]) are in bold. Matches not in bold were based on visual inspection.

Components	Excitation Maxima (nm)	Emission Maxima (nm)	Other Studies	Description
1	<250 (330)	468	**C1 (Jørgensen et al., 2011)** **C1 (Kowalczuk et al., 2009)** **G1 (Murphy et al., 2011)** **C3 (Seredynska-Sobecka et al, 2011)** **C1 (Shutova et al., 2014)** **C1 (Stedmon and Markager, 2005b)** **C1 (Stedmon et al., 2007a)** **C1 (Tanaka et al., 2014)** **C1 (Yamashita et al., 2010b)**	humic-like, terrestrial
2	255 (280)	392	C3 (Stedmon and Markager, 2005a) C2 and C3 (Stedmon and Markager, 2005b)	humic-like, terrestrial
3	280	340	**C7 (Murphy et al., 2008)** **C5 (Murphy et al. 2014a)**	Amino acids, free or bound in proteins
4	270	320	**C7 (Graeber et al., 2012)** **C4 (Yamashita et al., 2011)** **C3 (Yamashita et al., 2013)**	Protein- and tyrosine-like, positively related to bioavailability
5	<250	352	**C6 (Jørgensen et al., 2011)**	protein-like, resembles free tryptophan
6	<250 (325)	392	C4 (Jørgensen et al., 2011) C6 (Stedmon and Markager, 2005a) C2 (Stedmon et al., 2007a) C3 (Stedmon et al., 2007b) C2 (Yamashita et al., 2010a)	humic-like, marine also common in wastewater and agricultural catchments

Table 6. Fluorescence intensities (R.U.) of individual components identified using PARAFAC at the beginning and end of the 72 h irradiation. Percent of total fluorescence intensity is shown in parentheses.

Components	ICM_1	ICM_2	ICM_3	ICM_4	ICM_5	ICM_6	IFM_1	IFM_2	IFT_1	IFT_2
1	0.022 (13)	0.026 (21)	0.022 (16)	0.019 (17)	0.027 (20)	0.021 (16)	0.022 (6)	0.036 (25)	0.136 (40)	0.049 (29)
	0.017 (27)	0.019 (23)	0.016 (26)	0.018 (20)	0.025 (22)	0.024 (43)	0.017 (17)	0.021 (17)	0.060 (56)	0.044 (48)
2	0.008 (5)	0.018 (15)	0.008 (6)	0.013 (11)	0.019 (14)	0.029 (22)	0.001 (0)	0.015 (10)	0.063 (18)	0.029 (17)
	0.004 (7)	0.005 (6)	0.004 (6)	0.005 (5)	0.008 (7)	0.008 (15)	0.000 (0)	0.003 (2)	0.015 (14)	0.014 (15)
3	0.037 (22)	0.020 (16)	0.031 (22)	0.016 (15)	0.020 (14)	0.000 (0)	0.085 (22)	0.026 (18)	0.030 (9)	0.011 (7)
	0.018 (28)	0.023 (28)	0.007 (12)	0.007 (8)	0.021 (19)	0.002 (4)	0.031 (31)	0.031 (25)	0.007 (7)	0.005 (6)
4	0.036 (21)	0.032 (26)	0.032 (23)	0.028 (25)	0.030 (21)	0.074 (56)	0.075 (20)	0.029 (20)	0.035 (10)	0.030 (18)
	0.017 (25)	0.017 (20)	0.014 (24)	0.023 (26)	0.006 (5)	0.007 (12)	0.034 (34)	0.026 (21)	0.004 (4)	0.006 (7)
5	0.054 (32)	0.014 (11)	0.037 (27)	0.028 (25)	0.031 (23)	0.000 (0)	0.180 (48)	0.021 (15)	0.037 (11)	0.032 (19)
	0.001 (1)	0.010 (12)	0.013 (21)	0.027 (31)	0.039 (35)	0.003 (5)	0.010 (10)	0.031 (26)	0.001 (0)	0.005 (6)
6	0.011 (7)	0.014 (11)	0.010 (7)	0.007 (6)	0.012 (8)	0.014 (7)	0.014 (4)	0.016 (11)	0.044 (13)	0.018 (11)
	0.008 (12)	0.009 (11)	0.007 (11)	0.008 (9)	0.013 (11)	0.008 (20)	0.008 (9)	0.011 (9)	0.020 (19)	0.018 (19)

Figure Captions

Figure 1. Station locations for under-ice marine samples (white), ice-free marine samples (blue) and terrestrially-influenced samples (red). The location of the ice edge on the first day of sampling (July 3, 2011) and the last day of sampling (July 21, 2011) are indicated by the purple and blue lines respectively.

Figure 2. Loss of CDOM absorbance with irradiation for triplicate samples from experiments (a) ICM_1, (b) IFM_1 and (c) IFT_1. CDOM absorbance is shown at the start of the experiment (t_0) and after 4, 12, 24 and 72 hours (t_4, t_{12}, t_{24} and t_{72}).

Figure 3. Loss of CDOM absorbance at 254 nm as a function of (a) time and (b)the amount of cumulative UV light (280–400 nm) absorption at each time interval for all experiments.

Figure 4. Relationship between the initial CDOM absorption coefficient at 254 nm (C(0)) and the photoreactive component (z_0) from the three parameter exponential decay model.

Figure 5. Changes in the spectral slope $S_{275–295}$ (a) and $S_{350–400}$ (b) at each time interval for all experiments.

Figure 6. EEMs from a representative under-ice sample (ICM_1), ice-free marine sample (IFM_1), terrestrially-influenced sample (IFT_1), and a sample that shows protein-like production (IFT_2).

Formatted: Numbering: Continuous

Figure 7. The six-components for the PARAFAC model. The top two rows show the excitation (red lines) and emission (blue lines) loadings for each component and the bottom two rows show the individual components.

Figure 8. Variability in fluorescence for the six PARAFAC components for all experiments over the 72-hour irradiation experiments.

Figure 9. (a) Changes in CDOM absorbance at 254 nm as a function of the change in DOC after 72 hours for all experiments. (b) Percent loss in CDOM absorbance at 254 nm after 72 hours as a function of the percent loss in DOC for all experiments.

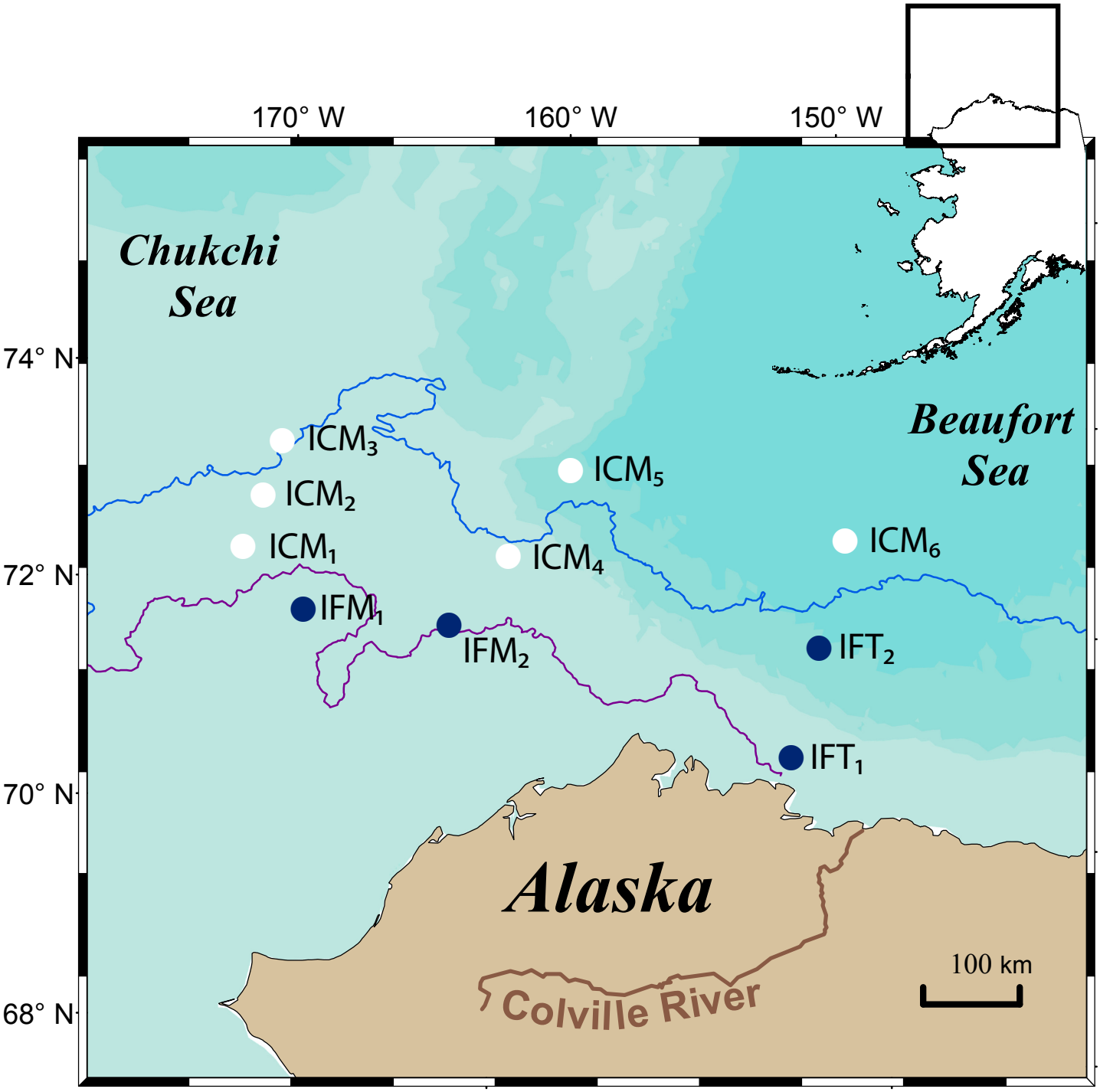
170° W
160° W
150° W
74° N
72° N
70° N
68° N
Chukchi Sea
Beaufort Sea
Alaska
Colville River
ICM3
ICM2
ICM1
ICM4
ICM5
ICM6
IFM1
IFM2
IFT2
IFT1
100 km

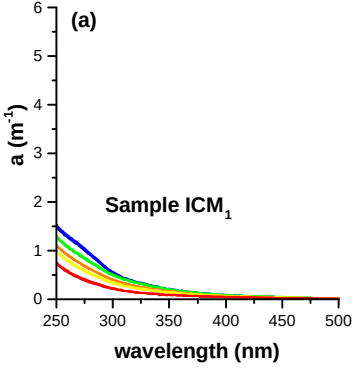
(a)
a (m-1)
Sample ICM1
wavelength (nm)
0
1
2
3
4
5
6
250
300
350
400
450
500

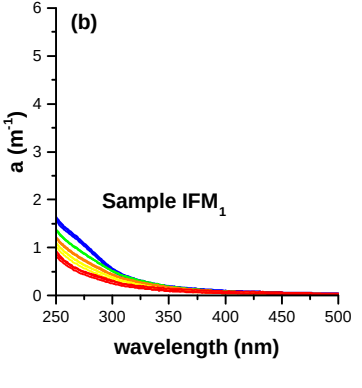
(b)
a (m-1)
Sample IFM1
wavelength (nm)
0
1
2
3
4
5
6
250
300
350
400
450
500

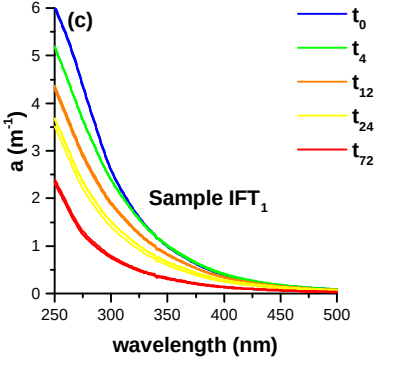
(c)
a (m-1)
Sample IFT1
wavelength (nm)
t0
t4
t12
t24
t72
0
1
2
3
4
5
6
250
300
350
400
450
500

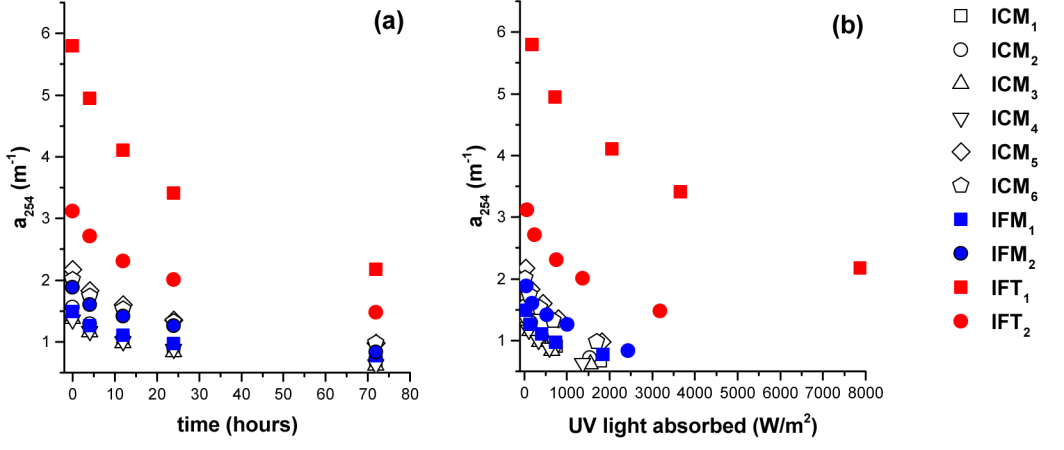
(a)
(b)
a_{254} (m^{-1})
time (hours)
UV light absorbed (W/m^2)
0
10
20
30
40
50
60
70
80
1000
2000
3000
4000
5000
6000
7000
8000
1
2
3
4
5
6
ICM$_1$
ICM$_2$
ICM$_3$
ICM$_4$
ICM$_5$
ICM$_6$
IFM$_1$
IFM$_2$
IFT$_1$
IFT$_2$

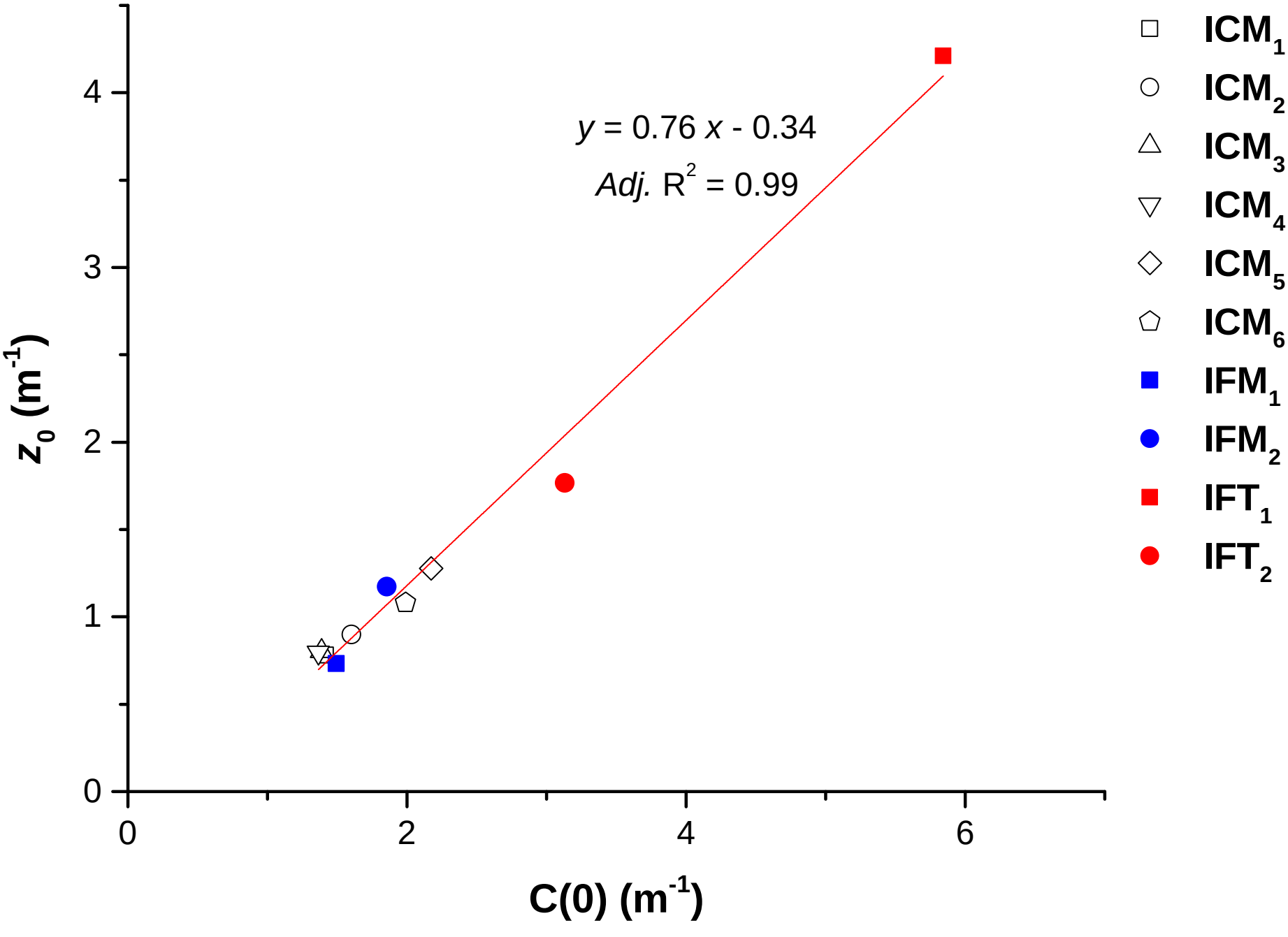
y = 0.76 x - 0.34
Adj. R2 = 0.99
z0 (m-1)
C(0) (m-1)
0
1
2
3
4
0
2
4
6
ICM1
ICM2
ICM3
ICM4
ICM5
ICM6
IFM1
IFM2
IFT1
IFT2

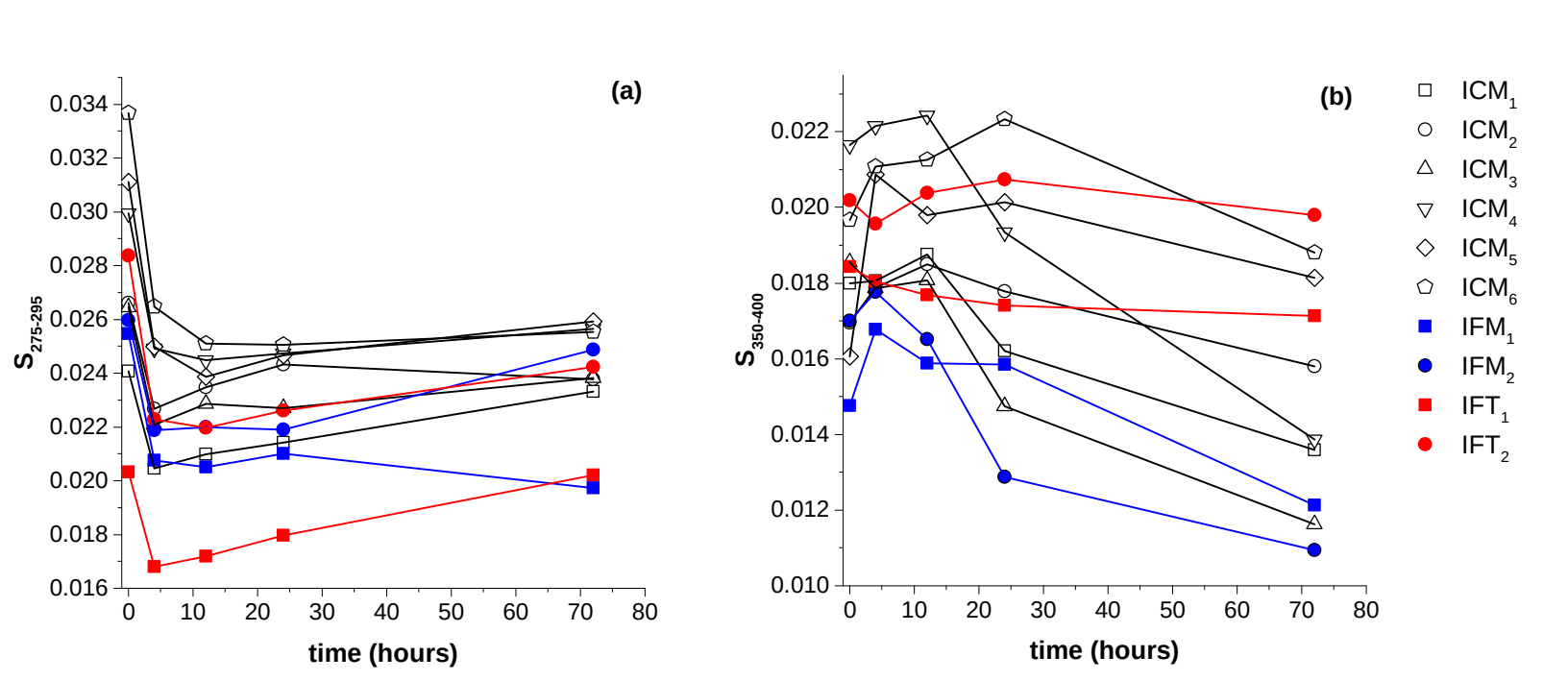
(a)
$S_{275-295}$
0.034
0.032
0.030
0.028
0.026
0.024
0.022
0.020
0.018
0.016
0
10
20
30
40
50
60
70
80
time (hours)
(b)
$S_{350-400}$
0.022
0.020
0.018
0.016
0.014
0.012
0.010
0
10
20
30
40
50
60
70
80
time (hours)
ICM_1
ICM_2
ICM_3
ICM_4
ICM_5
ICM_6
IFM_1
IFM_2
IFT_1
IFT_2

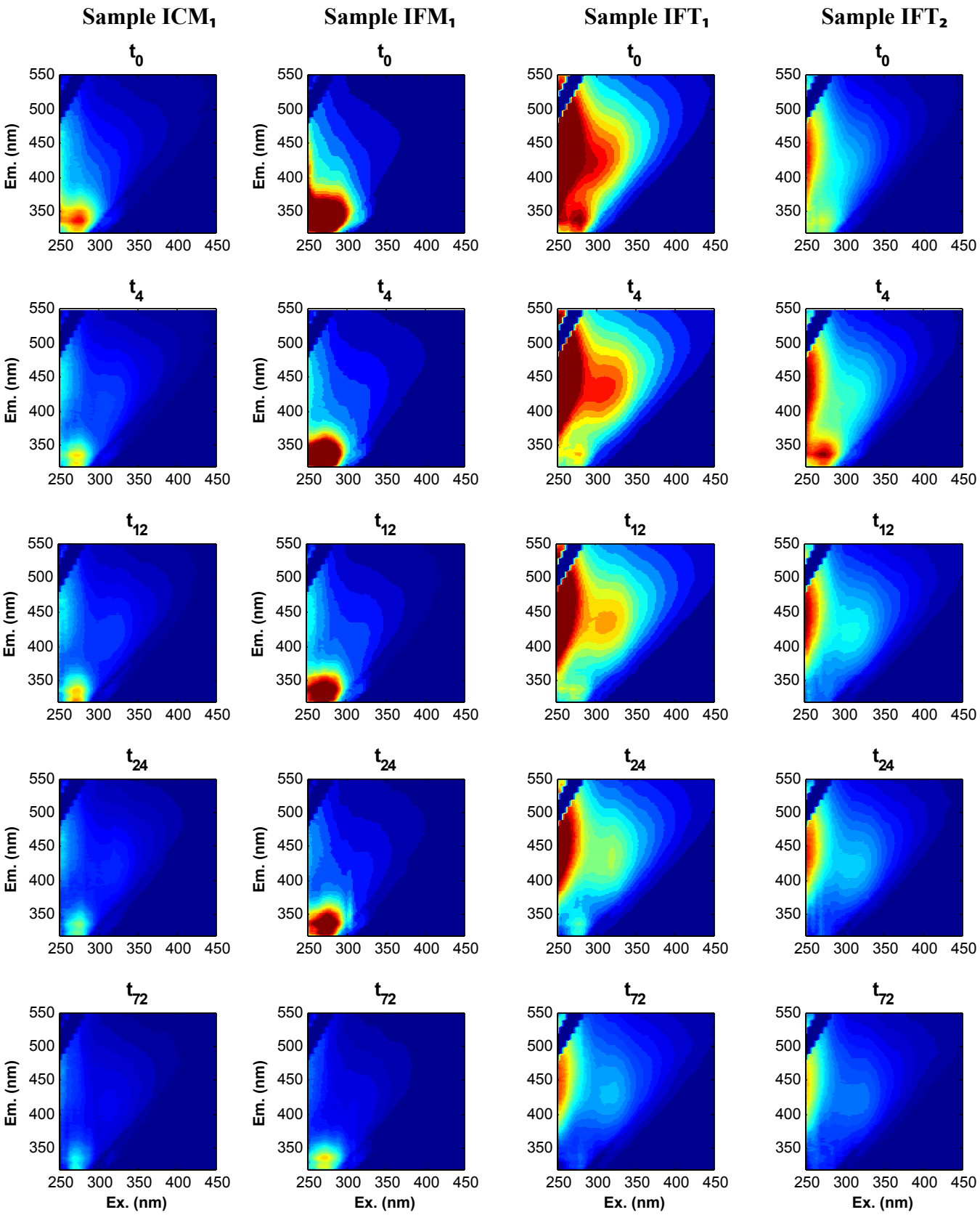
Sample ICM1
Sample IFM1
Sample IFT1
Sample IFT2
t0
t4
t12
t24
t72
Em. (nm)
Ex. (nm)
250 300 350 400 450
350 400 450 500 550

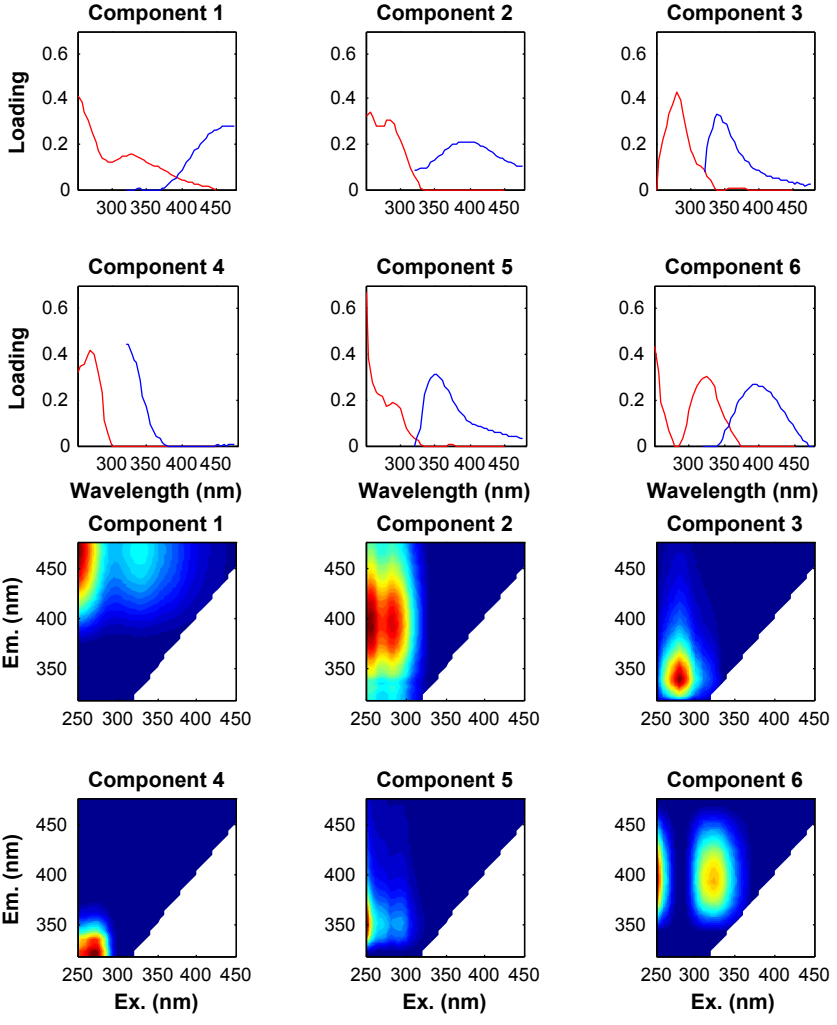
Component 1
Component 2
Component 3
Component 4
Component 5
Component 6
Loading
0.6
0.4
0.2
0
300 350 400 450
Wavelength (nm)
Em. (nm)
450
400
350
250 300 350 400 450
Ex. (nm)

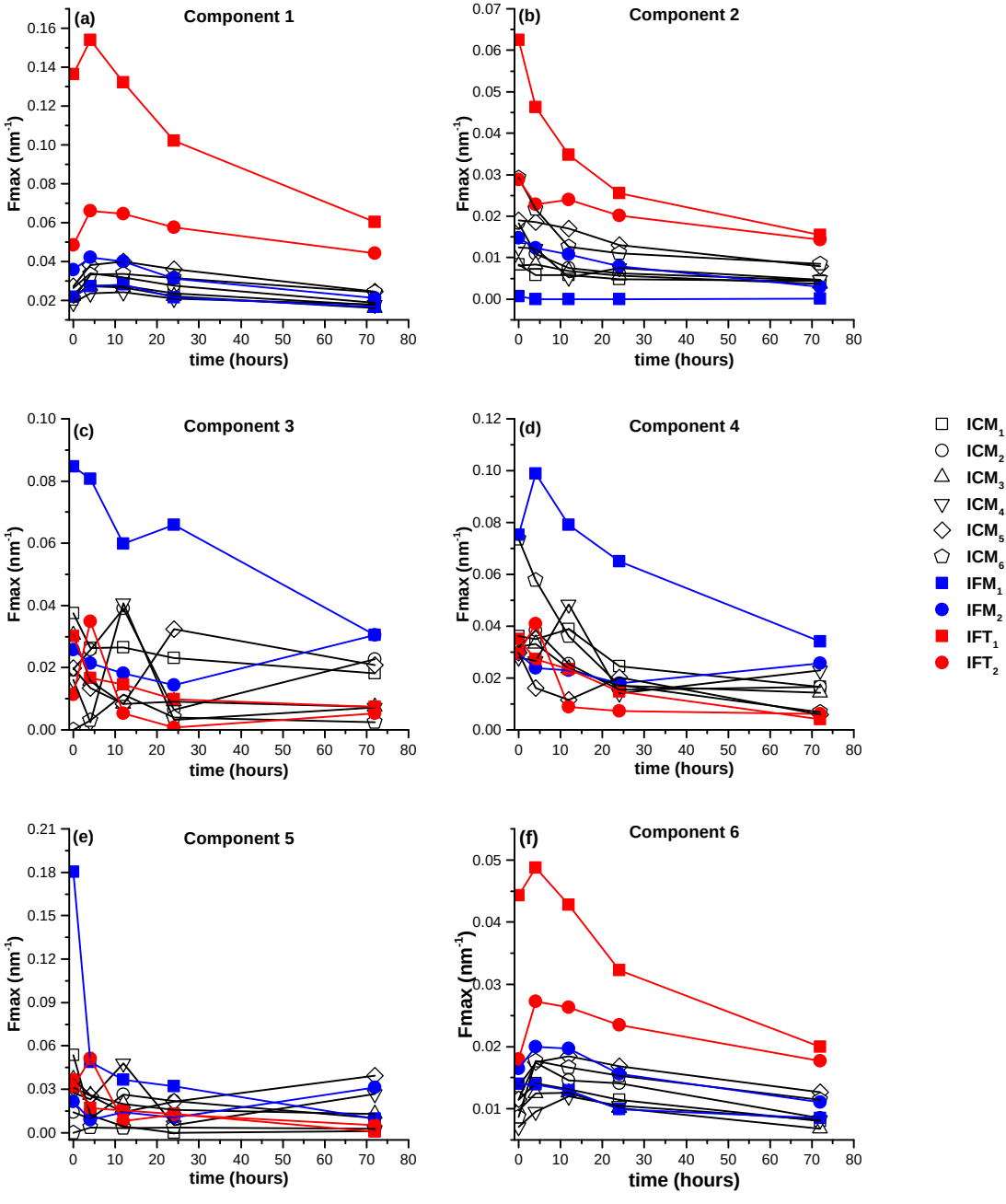
(a)
Component 1
Fmax (nm-1)
time (hours)
(b)
Component 2
Fmax (nm-1)
time (hours)
(c)
Component 3
Fmax (nm-1)
time (hours)
(d)
Component 4
Fmax (nm-1)
time (hours)
(e)
Component 5
Fmax (nm-1)
time (hours)
(f)
Component 6
Fmax (nm-1)
time (hours)
ICM1
ICM2
ICM3
ICM4
ICM5
ICM6
IFM1
IFM2
IFT1
IFT2

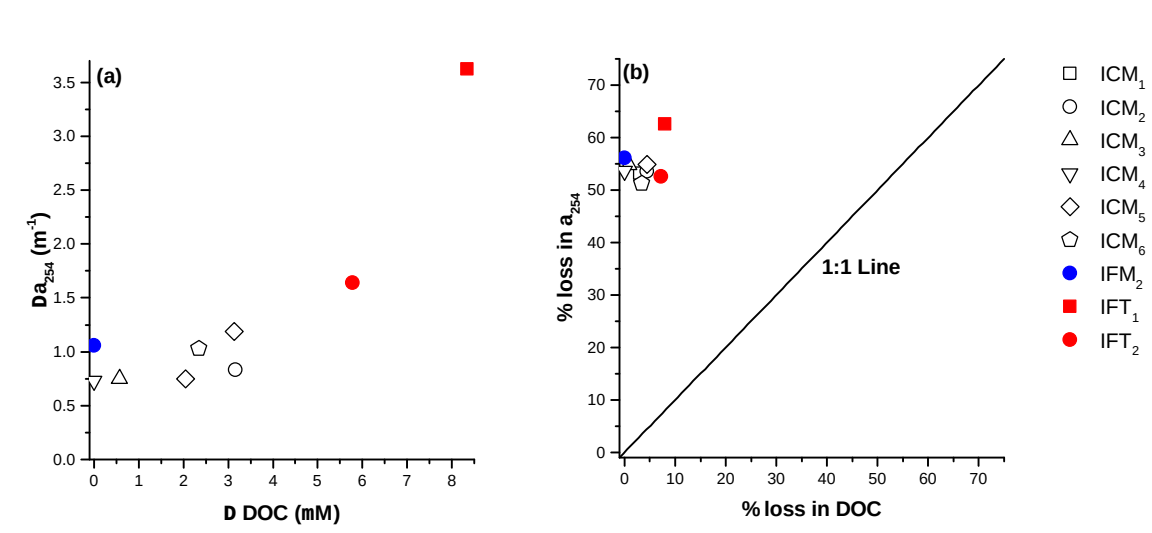
(a)
Da254 (m-1)
D DOC (mM)
0.0
0.5
1.0
1.5
2.0
2.5
3.0
3.5
0
1
2
3
4
5
6
7
8
(b)
% loss in a254
% loss in DOC
1:1 Line
0
10
20
30
40
50
60
70
ICM1
ICM2
ICM3
ICM4
ICM5
ICM6
IFM2
IFT1
IFT2